Magnetism in Fe-based superconductors



2010 J. Phys.: Condens. Matter 22 203203

(http://iopscience.iop.org/0953-8984/22/20/203203)

J. Phys.: Condens. Matter **22** (2010) 203203 (26pp) doi:10.1088/0953-8984/22/20/203203

## TOPICAL REVIEW

# Magnetism in Fe-based superconductors

**M D Lumsden and A D Christianson**

Neutron Scattering Science Division, Oak Ridge National Laboratory, Oak Ridge, TN 37831, USA

E-mail: lumsdenmd@ornl.gov and christiansonad@ornl.gov

Received 12 February 2010, in final form 7 April 2010
Published 30 April 2010
Online at stacks.iop.org/JPhysCM/22/203203

**Abstract**

In this review, we present a summary of experimental studies of magnetism in Fe-based superconductors. The doping dependent phase diagram shows strong similarities to the generic phase diagram of the cuprates. Parent compounds exhibit magnetic order together with a structural phase transition, both of which are progressively suppressed with doping, allowing superconductivity to emerge. The stripe-like spin arrangement of Fe moments in the magnetically ordered state shows identical in-plane structure for the RFeAsO (R = rare earth) and $AFe_2As_2$ (A = Sr, Ca, Ba, Eu and K) parent compounds, notably different than the spin configuration of the cuprates. Interestingly, $Fe_{1+y}Te$ orders with a different spin order despite having very similar Fermi surface topology. Studies of the spin dynamics of the parent compounds show that the interactions are best characterized as anisotropic three-dimensional interactions. Despite the room temperature tetragonal structure, analysis of the low temperature spin waves under the assumption of a Heisenberg Hamiltonian indicates strong in-plane anisotropy with a significant next-nearest-neighbor interaction. For the superconducting state, a resonance, localized in both wavevector and energy, is observed in the spin excitation spectrum as for the cuprates. This resonance is observed at a wavevector compatible with a Fermi surface nesting instability independent of the magnetic ordering of the relevant parent compound. The resonance energy ($E_r$) scales with the superconducting transition temperature ($T_C$) as $E_r \sim 4.9 k_B T_C$, which is consistent with the canonical value of $\sim 5 k_B T_C$ observed for the cuprates. Moreover, the relationship between the resonance energy and the superconducting gap, $\Delta$, is similar to that observed for many unconventional superconductors ($E_r/2\Delta \sim 0.64$).

(Some figures in this article are in colour only in the electronic version)

## Contents



## 1. Introduction

The discovery of superconductivity in F doped LaFeAsO with $T_C$ of 26 K [1] created a flurry of excitement in the condensed matter physics community. Substitutional replacement of the rare earth ion led to a rapid increase in the superconducting transition temperature. Denoting the chemical formula of these so-called 1111 materials by RFeAsO, F doping resulted in the following optimal transition temperatures: 52 K for

 

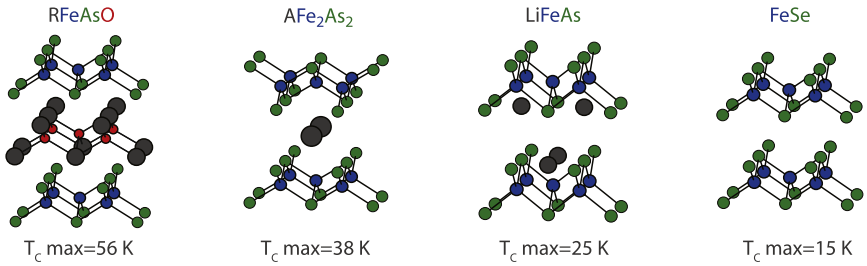


**Figure 1.** Crystal structure of the 1111, 122, 111, and 11 materials. In all cases, the FeAs (or FeSe) plane is the same with the principle difference being the spacer between layers. Below each figure is the maximum $T_C$ observed at ambient pressure in each of the families. From the figure, it is clear that the larger the separation between layers, the higher the transition temperature. (Figure courtesy M A McGuire).

R = Nd [2], 52 K for R = Pr [3], 55 K for R = Sm [4], 41 K for R = Ce [5], 36–50 K for R = Gd [6–8], 46 K for R = Tb [9], and 45 K for R = Dy [9]. To date, the highest transition temperature for the Fe-based superconductors is 56 K observed in a sample of $Gd_{1-x}Th_xFeAsO$ [10]. These superconducting transition temperatures make the Fe-based materials second only to the cuprates and they, therefore, represent the second family of high-$T_C$ superconductors. It was later shown that F doping was not necessary and similar transition temperatures could be obtained for the case of oxygen deficient $RFeAsO_{1-y}$: 28 K for R = La [11, 12], 42 K for Ce [11], 53 K for Nd [11–13], 48 K for Pr [11, 12], 55 K for Sm [11], 53 K for Gd [14, 12], 52 K for Tb and Dy [12]. Both the F doped and oxygen deficient samples show the same trend for $T_C$ as a function of rare earth ion.

At room temperature, the RFeAsO materials crystallize in the $P4/nmm$ tetragonal space group resulting in a layered structure with FeAs and RO layers [15] (see figure 1). This layered structure is reminiscent of the cuprates with FeAs planes taking the place of the CuO layers. The square planar arrangement of (likely) magnetic Fe is similar to the cuprates and leads one to naturally speculate that magnetism may play as essential role in the superconducting pairing. Shortly after the initial activity on the 1111 materials, superconductivity was also discovered in related materials possessing identical FeAs layers with differing spacers. The discovery of superconductivity with $T_C$ of 38 K in $Ba_{1-x}K_xFe_2As_2$ [16] was of particular interest as it was quickly realized that large single crystals of these 122 materials could be grown (unlike the 1111 family). Structurally, at room temperature, the 122 materials exhibit the $ThCr_2Si_2$ crystal structure (space group $I4/mmm$). As is clearly shown in figure 1, the FeAs layers are very similar to the 1111 materials although neighboring layers along the $c$-axis have an inverted arsenic coordination. For both the 1111 [17] and 122 [18] materials, it was quickly realized that replacement of Fe with Co would also result in superconductivity, albeit with a reduced $T_C$ when compared with doping between FeAs planes. Such behavior is in contrast to that observed in the cuprates where disorder in the copper oxide plane was found to destroy superconductivity. Superconductivity was also discovered in the 122 materials upon electron doping on the Fe site with Ni [19], Rh [20, 21], Ir [21] and Pd [20, 21] or by isoelectronic replacement of Fe with Ru [22, 23] (the resulting transition temperatures are shown in table 1). Interestingly, electron doping with Cu [24] or hole doping with Cr [25] does not yield superconductivity. The large number of potential dopants together with the availability of single crystal samples has made the 122 family of compounds the topic of considerable experimental focus.

Superconductivity was also discovered in LiFeAs [37–39] and $Na_{1-x}FeAs$ [40] (111 materials) sharing the same FeAs plane with Li or Na as the spacer as shown in figure 1. Transition temperatures of 18 K (for LiFeAs) and 12–25 K (for $Na_{1-x}FeAs$) [40] have been observed dependent on the precise Na concentration. Interestingly, superconductivity seems to appear in the 111 materials in purely stoichiometric material without chemical doping. Finally, the Fe(Se, Te) family of compounds (11 materials) also exhibits superconductivity with a maximum transition temperature (under ambient pressure) of 15 K. The alpha phase of FeSe is a superconductor with a transition temperature of 8 K [42]. Structurally, the FeSe plane is very similar to the FeAs plane in the aforementioned materials (see figure 1) indicating that the presence of As is not a requirement for superconductivity. Band structure calculations [43] suggested that FeTe may have enhanced superconducting properties. However, pure FeTe is not a superconductor [41] but is complicated by the presence of excess Fe, i.e. the actual chemical formula is $Fe_{1+y}Te$ [44]. It has been suggested that this excess Fe is magnetic and may act as a pair breaking moment destroying superconductivity [45]. Nonetheless, the doped material, $Fe_{1+y}Te_{1-x}Se_x$ does exhibit an enhanced $T_C$ of 15 K with the maximum transition temperature observed for $x$ near 0.5 [41].

The structures of the 1111, 122, 111, and 11 families of materials are shown in figure 1. The common feature is the presence of an identical FeAs (or FeSe) plane. An interesting trend can be seen in figure 1—the larger the separation between layers, the higher the observed optimal transition temperature. Two-dimensional (2D) magnetism occurs in the regions of highest $T_C$ and, thus, may be favorable for superconductivity. This trend led to attempts at further separating the FeAs layers and superconductivity with fairly high transition temperatures have been observed in $Sr_2VO_3FeAs$ with a spacer of $Sr_2VO_3$ and $T_C$ of 37.2 K [46], and doped $Sr_2Sc_{0.4}Ti_{0.6}FeAsO_3$ with a spacer of $Sr_2Sc_{0.4}Ti_{0.6}O_3$ and $T_C$ onset of 45 K (although the resistivity does not reach zero until ∼7 K) [47]. Although these temperatures still do not exceed the 56 K in the 1111 materials, they are quite high particularly in the case of $Sr_2VO_3FeAs$ as this material is nominally stoichiometric. There is hope that doping of this and related materials could lead to an increase in transition temperature.

**Table 1.** Summary of the maximum transition temperatures at ambient pressure for various Fe-based superconductors.

| Material | Max. $T_C$ (K) | Material | Max. $T_C$ (K) |
|---|---|---|---|
| $LaFeAsO_{1-x}F_x$ [1] | 26 | $Ba_{1-x}K_xFe_2As_2$ [16] | 38 |
| $NdFeAsO_{1-x}F_x$ [2] | 52 | $Ba_{1-x}Rb_xFe_2As_2$ [29] | 23 |
| $PrFeAsO_{1-x}F_x$ [3] | 52 | $K_{1-x}Sr_xFe_2As_2$ [30] | 36 |
| $SmFeAsO_{1-x}F_x$ [4] | 55 | $Cs_{1-x}Sr_xFe_2As_2$ [30] | 37 |
| $CeFeAsO_{1-x}F_x$ [5] | 41 | $Ca_{1-x}Na_xFe_2As_2$ [31] | 20 |
| $GdFeAsO_{1-x}F_x$ [7] | 50 | $Eu_{1-x}K_xFe_2As_2$ [32] | 32 |
| $TbFeAsO_{1-x}F_x$ [9] | 46 | $Eu_{1-x}Na_xFe_2As_2$ [33] | 35 |
| $DyFeAsO_{1-x}F_x$ [9] | 45 | $Ba(Fe_{1-x}Co_x)_2As_2$ [18, 34] | 22–24 |
| $Gd_{1-x}Th_xFeAsO$ [10] | 56 | $Ba(Fe_{1-x}Ni_x)_2As_2$ [19] | 20 |
| $LaFeAsO_{1-y}$ [11, 12] | 28 | $Sr(Fe_{1-x}Ni_x)_2As_2$ [35] | 10 |
| $NdFeAsO_{1-y}$ [11–13] | 53 | $Ca(Fe_{1-x}Co_x)_2As_2$ [36] | 17 |
| $PrFeAsO_{1-y}$ [11, 12] | 48 | $Ba(Fe_{1-x}Rh_x)_2As_2$ [20] | 24 |
| $SmFeAsO_{1-y}$ [11] | 55 | $Ba(Fe_{1-x}Pd_x)_2As_2$ [20] | 19 |
| $GdFeAsO_{1-y}$ [14, 12] | 53 | $Sr(Fe_{1-x}Rh_x)_2As_2$ [21] | 22 |
| $TbFeAsO_{1-y}$ [12] | 52 | $Sr(Fe_{1-x}Ir_x)_2As_2$ [21] | 22 |
| $DyFeAsO_{1-y}$ [12] | 52 | $Sr(Fe_{1-x}Pd_x)_2As_2$ [21] | 9 |
| $LaFe_{1-x}Co_xAsO$ [17] | 14 | $Ba(Fe_{1-x}Ru_x)_2As_2$ [22] | 21 |
| $SmFe_{1-x}Ni_xAsO$ [26] | 10 | $Sr(Fe_{1-x}Ru_x)_2As_2$ [23] | 13.5 |
| $SmFe_{1-x}Co_xAsO$ [27] | 15 | LiFeAs [37–39] | 18 |
| $LaFe_{1-x}Ir_xAsO$ [28] | 12 | $Na_{1-x}FeAs$ [40] | 25 |
| | | $Fe_{1+y}Se_xTe_{1-x}$ [41] | 15 |

Shortly after the discovery of superconductivity in $LaFeAsO_{1-x}F_x$, calculations indicated that conventional electron–phonon coupling was insufficient to explain the high transition temperatures [48], as was later verified experimentally [49]. As will be explained below, a ubiquitous magnetically ordered state is present indicating magnetism in close proximity to superconductivity leading one to naturally consider the interplay between magnetism and superconductivity in these materials. In the following article, we will review *experimental* studies of magnetism in the Fe-based compounds and its influence on superconductivity.

## 2. Phase Diagrams

### *2.1. 1111 materials*

The first evidence for the importance of magnetism in the Fe-based superconductors was the concentration dependent phase diagram presented with the initial discovery of superconductivity in F doped LaFeAsO [1]. An additional phase was clearly present at low F concentration which vanished at doping levels where superconductivity appears although the exact nature of this phase was unclear. It was soon shown that the undoped LaFeAsO parent compound exhibited spin-density wave (SDW) order below about 150 K [15, 50] consistent with a $\sqrt{2} \times \sqrt{2} \times 2$ unit cell. Unexpectedly, LaFeAsO also exhibited a structural phase transition [15] at a temperature slightly above the magnetic ordering temperature. The low temperature structure was originally described by the monoclinic $P112/n$ space group [15] but it was later clarified that the correct low temperature space group is the orthorhombic $Cmma$ [51] (note that both notations accurately describe the observed structure). There is clear competition between magnetism and superconductivity as the magnetically ordered state is destroyed in the fluorine doped, superconducting samples [15, 50].

The phase diagram of $RFeAsO_{1-x}F_x$ as a function of doping has been carefully studied for R = La [52] (figure 2(a)), Ce [53] (figure 2(b)), Pr [56] and Sm [54, 57] (figure 2(c)). The phase diagrams were experimentally determined using the following techniques: R = La, $\mu$SR, $^{57}$Fe Mössbauer spectroscopy and x-ray diffraction [52]; R = Ce, neutron diffraction, resistivity and magnetization [53]; R = Pr, x-ray diffraction, resistivity and magnetization [56]; R = Sm, $\mu$SR [54] and x-ray diffraction [57]. For R = Nd, a partial phase diagram [58] was determined using resistivity measurements. In all cases measured, the $x = 0$ parent compounds show a structural phase transition at a temperature slightly above the transition to magnetic ordering with a typical structural transition at ∼150 K and SDW ordering at about 140 K. In general, doping causes a suppression of both the structural and magnetic phase transitions and as these are suppressed, superconductivity emerges. The fundamental difference between materials with different rare earths comes in the behavior near the emergence of superconductivity. For R = La and Pr, the structural and magnetic transitions vanish in an abrupt step-like manner as a function of doping at the onset of superconductivity [52, 56], as shown in figure 2(a) for the case of R = La. For the case of R = Ce, the magnetic transition appears to vanish continuously to very low temperatures and superconductivity emerges at a concentration where this transition has been completely suppressed [53] (see figure 2(b)). However, the structural transition has some range of concentrations where superconductivity coexists with this phase transition [53]. Finally, the case or R = Sm, shown in figure 2(c), looks similar to R = Ce in that the transitions are suppressed gradually and there appears to be overlap between the structural transition and superconductivity [57]. However, unlike the case of Ce, the Sm phase diagram shows a region where magnetic ordering coexists with superconductivity [54]. This suggests that the destruction of long range magnetic

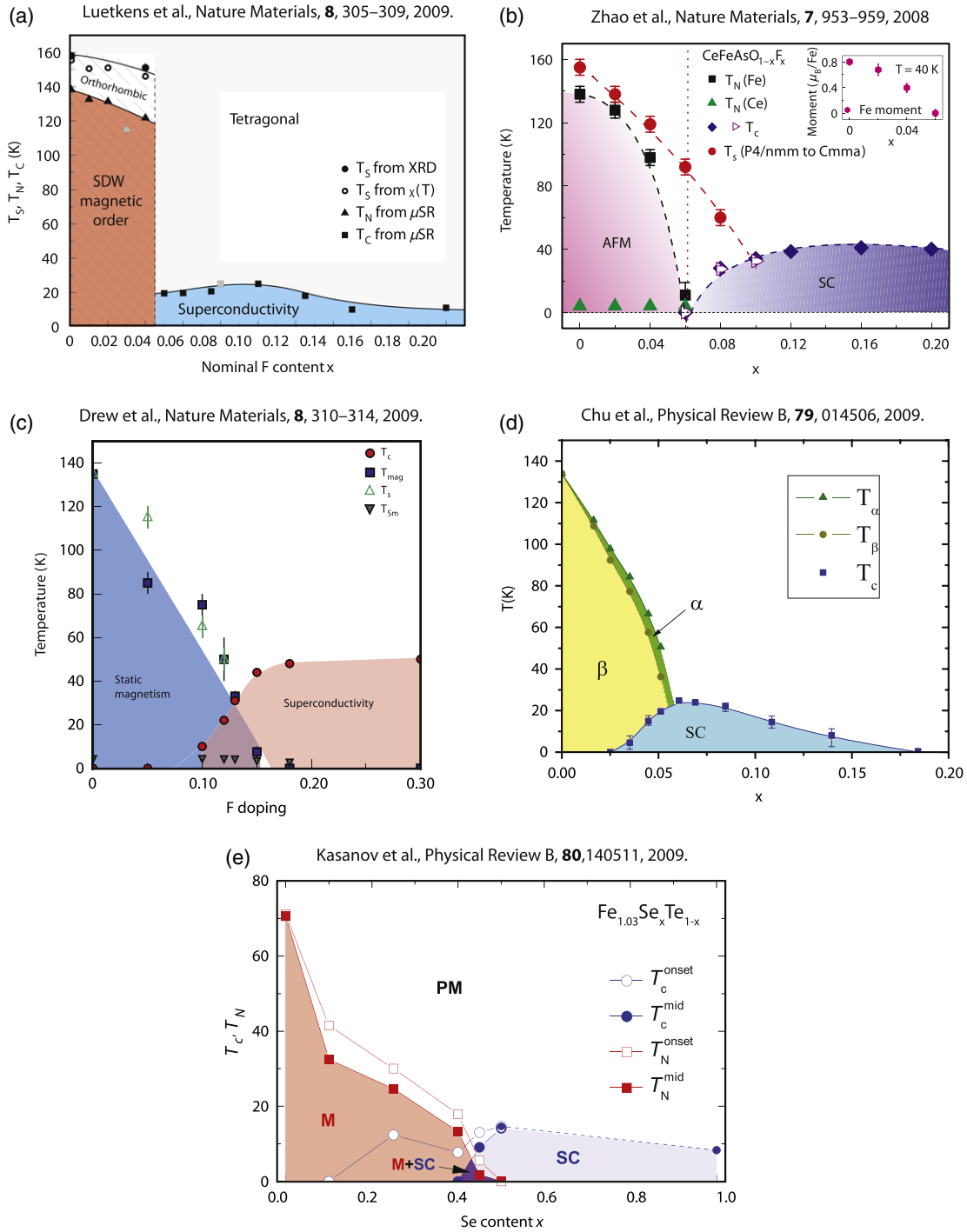


**Figure 2.** Experimentally determined phase diagram for (a) $LaFeAsO_{1-x}F_x$ (reprinted by permission from Macmillan publishers Ltd: Nature Materials [52], copyright 2009), (b) $CeFeAsO_{1-x}F_x$ (reprinted by permission from Macmillan publishers Ltd: Nature Materials [53], copyright 2008), (c) $SmFeAsO_{1-x}F_x$ (reprinted by permission from Macmillan publishers Ltd: Nature Materials [54], copyright 2009), (d) $BaFe_{2-x}Co_xAs_2$ (reprinted with permission from [34], copyright 2009 the American Physical Society), and (e) $Fe_{1.03}Te_{1-x}Se_x$ (reprinted with permission from [55], copyright 2009 the American Physical Society).

order is not a necessary condition for the emergence of superconductivity.

### 2.2. 122 materials

As mentioned previously, and shown in table 1, the $AFe_2As_2$ family of materials has numerous doping possibilities. The basic behavior of the superconducting materials can be described by considering the phase diagrams for $Ba_{1-x}K_xFe_2As_2$ (hole doping between the FeAs planes) and $BaFe_{2-x}Co_xAs_2$ (electron doping within the FeAs plane). Both materials share the same $BaFe_2As_2$ parent compound. As in the case of the 1111 parent compounds, Ba-122 exhibits

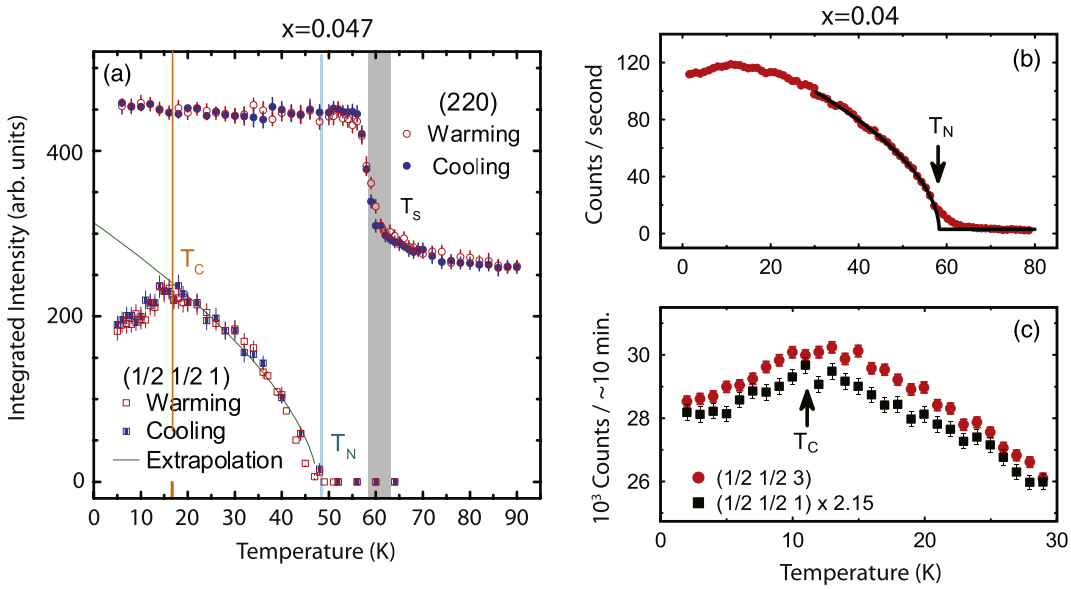


**Figure 3.** Suppression of the magnetic Bragg peak intensity on entering the superconducting state for $Ba(Fe_{0.953}Co_{0.047})_2As_2$ ($x = 0.047$) (reprinted with permission from [66], copyright 2009 the American Physical Society) and $Ba(Fe_{0.96}Co_{0.04})_2As_2$ ($x = 0.04$) (reprinted with permission from [67], copyright 2009 the American Physical Society).

both a structural phase transition (in this case from the room temperature tetragonal $I4/mmm$ space group to the low temperature orthorhombic $Fmmm$ space group [59, 60]) and the magnetic transition to a long range ordered, SDW state. However, unlike the 1111 materials, both the structural and magnetic phase transitions occur at the same temperature in the Ba-122 parent compound [59–61]. Doping with either K [62, 63] or Co [34, 64, 65] causes a suppression of the structural and SDW transitions as in the 1111 materials. For Co doping, as $x$ increases, the two transitions no longer appear at the same temperature with the structural transition occurring first upon cooling [64] as shown in figure 2(d). In both cases, superconductivity emerges as the SDW order is suppressed. For K doping, the superconducting region starts for $x \sim 0.1$ and the maximum $T_C$ of 38 K is reached for $x \sim 0.4$ [62, 63]. For $Ba(Fe_{1-x}Co_x)_2As_2$, superconductivity is first observed for $x \sim 0.03$ and the maximum $T_C$ of 23 K is seen for $x \sim 0.07$ [34, 65]. Interestingly, for both K and Co doping, there is a region of the phase diagram where the SDW state and structural transition coexist with superconductivity.

Coexistence of superconductivity and magnetism has been a recurring theme in the study of superconducting materials [68–71]. For the doped 122 materials, the question of whether the SDW and superconducting states are microscopically coexisting or phase separated has received considerable attention experimentally. For hole doping with K, $^{75}$As NMR [72], $\mu$SR [73] and magnetic force microscopy [73] consistently indicate distinct regions which are magnetically ordered and nonmagnetic regions as expected for microscopic phase separation. Furthermore, analysis of microstrain measured with x-ray and neutron diffraction was interpreted as being consistent with electronic phase separation [74]. Although most measurements on the K doped samples are consistent with a phase separation scenario, $^{57}$Fe-Mössbauer measurements indicate a sample which is completely magnetically ordered as expected with microscopic coexistence of the SDW and superconducting states [75]. For the case of Co doping, both $^{75}$As NMR [76] and $\mu$SR measurements [77] indicate that all the Fe sites participate in the magnetic order as would be expected for coexistence of superconductivity and SDW order. One $^{75}$As NMR study directly compared the cases of K and Co doping and concluded phase coexistence for Co doped samples and separation for the case of K doping [78]. Finally, we note neutron diffraction measurements on Co doped samples [66, 67] showed that the magnetic Bragg peak intensity of the SDW state is suppressed on entering the superconducting state, as shown in figure 3, for $x = 0.04$ and 0.047. This certainly shows a very strong interaction between the superconducting and SDW states. It could be interpreted that this suppression is due to the same electrons participating in both the SDW and superconductivity favoring a phase coexistence scenario. However, in a phase separation scenario, a proximity effect could cause the superconducting regions to interfere with the SDW regions causing a reduction in the SDW volume consistent with the observed Bragg peak intensity reduction. Hence, it is difficult to make any strong conclusions about the implications of this observation for the question of phase coexistence.

Interestingly, the details of the phase diagram in the region where the structural and magnetic transitions cross the superconducting dome have recently been explored with high resolution x-ray diffraction [79]. These measurements indicate that the shape of the line in the $x$–$T$ phase diagram representing the tetragonal to orthorhombic transition changes on entering the superconducting state and bends to lower values of $x$ [79] as shown in figure 4(a). As such, clear reentrant behavior is seen in a crystal of $Ba(Fe_{0.938}Co_{0.062})_2As_2$ where the system transforms from tetragonal to orthorhombic and back to tetragonal on cooling [79] (see figure 4(b)). This

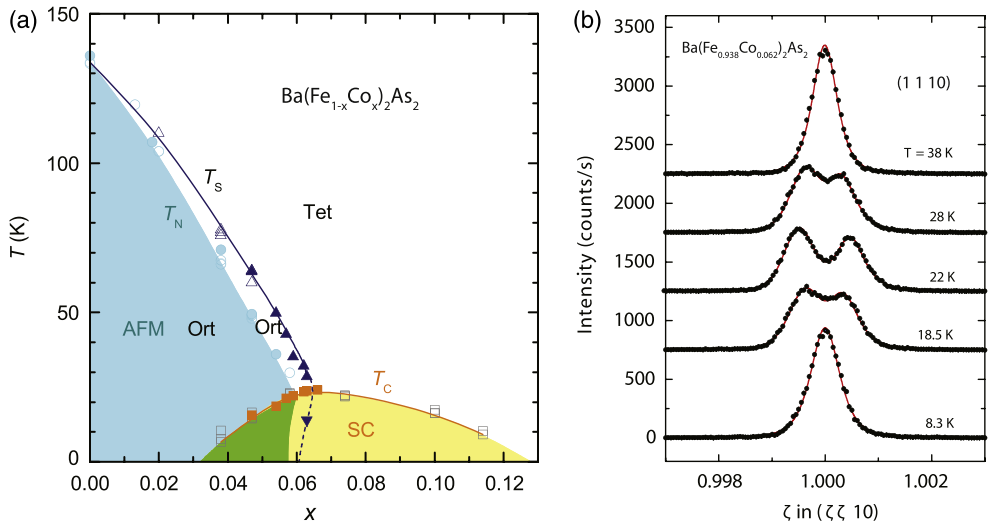


**Figure 4.** (a) Resulting phase diagram of $Ba(Fe_{1-x}Co_x)_2As_2$ with inclusion of high resolution x-ray diffraction measurements in the region where superconductivity and magnetism coexist [79]. (b) Shows the reentrant nature of the structural phase transition. (Reprinted with permission from [79], copyright 2010 the American Physical Society.)

shows a strong interaction between the structural transition and superconductivity and it was proposed that the interaction was actually one between magnetism and superconductivity with the influence on the structural transition resulting from magneto-elastic coupling [79].

### *2.3. 11 materials*

Finally, we discuss the phase diagram of the $FeSe_xTe_{1-x}$ family of materials. As mentioned previously, these materials form with excess Fe with the largest amount of extra Fe observed near the Te-rich side of the phase diagram. Initial measurements of the $Fe_{1+y}Te_{1-x}Se_x$ [41] family of compounds showed superconductivity with $T_C$ as high as 15 K for $x \sim 0.5$ existing for all values of $x$ except very near $x = 0$ where superconductivity is destroyed. This suggests a different phase diagram from other Fe-based superconductors. However, single crystal specific heat measurements on the Te-rich side of the phase diagram indicate bulk superconductivity only for concentrations near $x = 0.5$ [80]. With this in mind, the phase diagram was reinvestigated and indicated magnetic order for small $x$ which coexists with superconductivity over a range of concentrations [55] (see figure 2(e)) in a manner very similar to the doped 122 materials and $SmFeAsO_{1-x}F_x$. As mentioned previously, materials with low Se concentrations have a tendency to form with excess Fe. Measurements of the phase diagram with samples intentionally grown with $Fe_{1.1}$ [81] show an additional spin glass phase which coexists with superconductivity over much of the measured concentration range. This shows the sensitivity of these materials to stoichiometry and, in particular, the amount of excess Fe present.

Although, as discussed above, there are some differences in the concentration dependent phase diagrams of various Fe-based superconductors, inspection of figure 2 shows that there are some common features. All materials exhibit a SDW state at low concentrations and this state is suppressed with doping allowing for the emergence of superconductivity. This shows strong similarity to the generic cuprate phase diagram and is evidence for the interplay of magnetism and superconductivity in the Fe-based materials.

## 3. Magnetic order

The parent compounds of both the 1111 and 122 materials are metals which exhibit SDW order. The high temperature ($T > T_N$) paramagnetic state is characterized by magnetic susceptibility with an unusual linear temperature dependence ($\chi \propto T$) [82, 31, 83–86]. This behavior is neither Pauli- nor Curie–Weiss-like and is reminiscent of the ($T > T_{SDW}$) behavior of metallic Cr [87]. In the following section, we will provide an overview of the magnetic order which evolves out of this unusual paramagnetic state in the 1111, 122, and 11 family of materials. Examination of the magnetic ordering can shed light on the magnetic interactions and the nature (local moment or itinerant) of the magnetism in these materials.

### *3.1. 1111 materials*

As discussed above, it is well established that the undoped parent compounds exhibit some form of antiferromagnetic long range order. This was first observed in LaFeAsO where the magnetic structure was characterized by the ordering wavevector $(\frac{1}{2}\ \frac{1}{2}\ \frac{1}{2})_T = (1\ 0\ \frac{1}{2})_O$ (where the subscripts T and O refer to the tetragonal and orthorhombic structures, respectively) and the low temperature ordered magnetic moment was 0.36 $\mu$B [15]. At this point, we note that the ordering wavevector in the orthorhombic cell (i.e. $(1\ 0\ \frac{1}{2})_O$) differs from the wavevector listed in [15] as the later wavevector is relative to the unit cell of the magnetic structure where the unit cell is doubled along the $c$-axis. The observed wavevector is consistent with a magnetic unit cell of size $\sqrt{2}a \times \sqrt{2}a \times 2c$ relative to the tetragonal cell. This

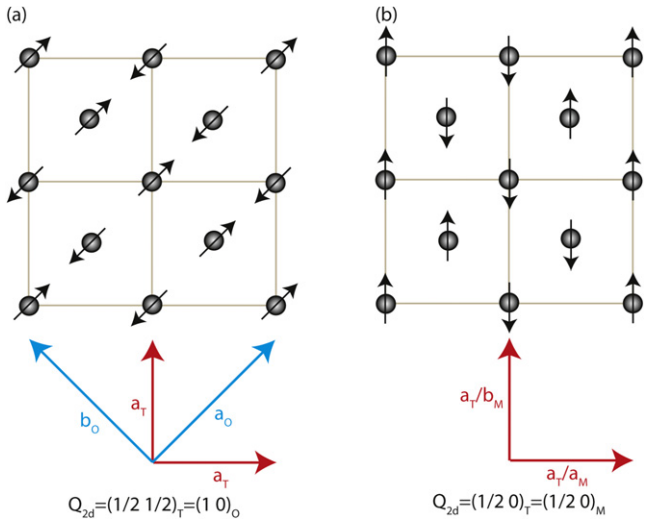


**Figure 5.** (a) In-plane magnetic structure for the 1111 and 122 parent compounds. The ordering wavevector in these compounds is $(\frac{1}{2}\ \frac{1}{2}\ L)_T = (1\ 0\ L)_O$. For the 1111 materials, the stacking of neighboring plane along the $c$-axis is either ferromagnetic or antiferromagnetic depending on the rare earth element (see table 2). For the 122 materials, the stacking is antiferromagnetic along the $c$-axis resulting in odd-integer $L$ as the unit cell contains two FeAs layers. (b) Magnetic structure for 11 materials ($Fe_{1+x}Te$) in the limit of smaller $x$ where the low temperature nuclear structure is monoclinic. The ordering wavevector is $(\frac{1}{2}\ 0\ \frac{1}{2})$ and is the same in both the high and low temperature phases.

ordering is consistent with stripe-like antiferromagnetic order with ferromagnetically coupled chains along the tetragonal (110) direction coupled antiferromagnetically along the in-plane perpendicular direction (see figure 5(a)). The doubling of the unit cell along the $c$-axis indicates antiferromagnetic interactions between neighboring planes. The magnetic moment direction could not be uniquely determined in this measurement but the observed intensity is consistent with moments lying in the $a$–$b$ plane. The magnetic moment observed is much smaller than the 2.2 $\mu$B moment observed in metallic Fe. Measurements of $LaFeAsO_{1-x}F_x$ shows that the magnetic moment is rather independent of concentration for $x < 0.03$ and is zero for $x > 0.05$ [88]. More concentration points are required to determine how abruptly the magnetic moment vanishes with fluorine concentrations between 3 and 5%.

The nature of the ordered state in these materials has been a topic of considerable study. The calculated Fermi surface for LaFeAsO consists of electron cylinders near the M point and hole cylinders and a 3D hole pocket around the Γ point [89]. Further investigations indicated good nesting of these components separated by the 2D wavevector $(\frac{1}{2}\ \frac{1}{2})_T$ consistent with the observed magnetic structure [90, 91]. This led to the suggestion that the observed antiferromagnetic state is a SDW induced by Fermi surface nesting [91]. In addition to this Fermi surface nesting scenario, it has been proposed that near-neighbor and next-near-neighbor interactions between local Fe moments are both antiferromagnetic and of comparable strength leading to magnetic frustration [92–94]. In addition to describing the observed magnetic structure, this scenario can also provide an explanation for the structural phase transition as the lattice distortion relieves the magnetic frustration [92, 93]. These frustration effects have also been used to explain the small ordered moment [92, 94]. Starting with a local moment Hamiltonian consistent with those discussed previously [92–94], it was suggested that the structural transition is actually a transition to a 'nematic' ordered phase which will occur at a higher temperature than the SDW transition [95]. In addition to the view that the magnetic order is driven exclusively by either Fermi surface nesting or local moment superexchange interactions, an alternate approach based on analysis of DFT calculations included aspects of both [96]. This work concluded that the moments were largely local in nature but the interactions were relatively long-ranged itinerant interactions as opposed to superexchange and both the low temperature magnetic order and structural distortions were explained [96]. Finally, it was recently proposed that both the magnetic and structural transitions are driven by orbital physics and that the structural transition is, in fact, a ferro-orbital ordering transition [97]. This model explains the coupling of the structural and magnetic transitions and is consistent with the rather large ordering temperature [97].

Changes of the ordered magnetic structure with different rare earth elements (RFeAsO) have been extensively studied with neutron diffraction as well as local probe methods. The ordering wavevector of $(\frac{1}{2}\ \frac{1}{2}\ \frac{1}{2})_T$ observed for R = La [15] is also observed for R = Nd [98]. However, for R = Ce [53] and R = Pr [99] the ordering is described by the wavevector $(\frac{1}{2}\ \frac{1}{2}\ 0)_T$ suggesting ferromagnetic coupling between planes. This suggests rather weak interplane coupling which is strongly influenced by the rare earth ion and the associated induced structural changes. Unfortunately, for the case of R = Sm, the high absorption cross-section for Sm makes neutron scattering measurements very difficult. Neutron scattering measurements on SmFeAsO were performed [100] but could only explore the low temperature ordering of the Sm moments as will be discussed below.

The size of the ordered moment as a function of R has been a topic of considerable interest. Neutron scattering on R = Pr indicates a moment of 0.34 $\mu$B [101] identical to that observed for R = La [15] (a moment of 0.48 $\mu$B [99] was independently observed but this was measured below the Pr ordering temperature). The moment for R = Nd appears smaller and initially, Fe ordering was not observed [102] with an upper bound on the ordered moment placed at 0.17 $\mu$B. However, later measurements clearly indicated Fe ordering with an ordered moment of 0.25 $\mu$B [98], the smallest of any of the rare earths. A particularly interesting case is that of Ce where neutron scattering indicated a much larger magnetic moment of 0.8 $\mu$B [53] more than twice the size of any other rare earth. Thus, on the basis of these neutron diffraction results, the Fe moment size varies considerably with rare earth element. However, a contradictory picture is obtained from $^{57}$Fe Mössbauer measurements. Such measurements for R = La indicate an internal magnetic field of 4.86 T [103], 5.19 T [50], and 5.3 T [104]. For the other rare earths, the internal field was measured to be 5.2 T [105] and 5.3 T [106]

**Table 2.** Magnetic structure parameters for Fe order. The ordered moment for $^{57}$Fe Mössbauer measurements is shown in units of internal magnetic field and can be converted to $\mu$B such that 15 T internal field corresponds to 1 $\mu$B [50, 106]. For $\mu$SR measurements, the ordered moment is presented as a saturation frequency in megahertz. Note that we characterize the magnetic structure in this table by an ordering wavevector relative to the respective (tetragonal or orthorhombic) nuclear cell. This differs from the wavevector listed in some references (for instance, [119]) where the characteristic wavevector is relative to a unit cell expanded to fully include the magnetic structure forcing all indices to be integer.

| Material | $T_N$ (K) | Wavevector | Moment | Technique | Reference |
|---|---|---|---|---|---|
| LaFeAsO | 137 | $(1\ 0\ \frac{1}{2})_O/(\frac{1}{2}\ \frac{1}{2}\ \frac{1}{2})_T$ | 0.36 $\mu$B | Neutrons | [15] |
| | 138 | | 4.86 T/23 MHz | Mössbauer/$\mu$SR | [103] |
| | 145 | | 5.19 T | Mössbauer | [50] |
| | 140 | | 5.3 T | Mössbauer | [104] |
| NdFeAsO | 141 | $(1\ 0\ \frac{1}{2})_O/(\frac{1}{2}\ \frac{1}{2}\ \frac{1}{2})_T$ | 0.25 $\mu$B | Neutrons | [98] |
| | 141 | | 5.3 T | Mössbauer | [106] |
| | 135 | | 23 MHz | $\mu$SR | [108] |
| PrFeAsO | 136 | $(1\ 0\ 0)_O/(\frac{1}{2}\ \frac{1}{2}\ 0)_T$ | 0.35 $\mu$B | Neutrons | [101] |
| | 139 | | 4.99 T | Mössbauer | [106] |
| | 123 | | 23 MHz | $\mu$SR | [107] |
| CeFeAsO | 140 | $(1\ 0\ 0)_O/(\frac{1}{2}\ \frac{1}{2}\ 0)_T$ | 0.8 $\mu$B | Neutrons | [53] |
| | 136 | | 5.06 T | Mössbauer | [106] |
| | 137 | | ~26 MHz | $\mu$SR | [107] |
| SmFeAsO | 135 | | 23.6 MHz | $\mu$SR | [54] |
| $BaFe_2As_2$ | 90* | $(1\ 0\ 1)_O/(\frac{1}{2}\ \frac{1}{2}\ 1)_T$ | 0.99 $\mu$B | Neutrons | [110] |
| | 143 | $(1\ 0\ 1)_O/(\frac{1}{2}\ \frac{1}{2}\ 1)_T$ | 0.87 $\mu$B | Neutrons | [60] |
| | 140 | | 28.8 MHz | $\mu$SR | [108] |
| | 140 | | 5.47 T | Mössbauer | [108] |
| $SrFe_2As_2$ | 220 | $(1\ 0\ 1)_O/(\frac{1}{2}\ \frac{1}{2}\ 1)_T$ | 0.94 $\mu$B | Neutrons | [111] |
| | 205 | $(1\ 0\ 1)_O/(\frac{1}{2}\ \frac{1}{2}\ 1)_T$ | 1.01 $\mu$B | Neutrons | [112] |
| | 205 | | 44 MHz | $\mu$SR | [113] |
| | 205 | | 8.91 T | Mössbauer | [114] |
| $CaFe_2As_2$ | 173 | $(1\ 0\ 1)_O/(\frac{1}{2}\ \frac{1}{2}\ 1)_T$ | 0.8 $\mu$B | Neutrons | [115] |
| $EuFe_2As_2$ | 200 | | 8.5 T | Mössbauer | [116] |
| $Fe_{1.076}Te$ | 75 | $(\frac{1}{2}\ 0\ \frac{1}{2})$ | 2.03 $\mu$B | Neutrons | [44] |
| $Fe_{1.141}Te$ | 63 | $(0.38\ 0\ \frac{1}{2})$ | 1.96 $\mu$B | Neutrons | [44] |
| $Fe_{1.068}Te$ | 67 | $(\frac{1}{2}\ 0\ \frac{1}{2})$ | 2.25 $\mu$B | Neutrons | [117] |
| $Na_{1-\delta}FeAs$ | 37 | $(1\ 0\ \frac{1}{2})_O/(\frac{1}{2}\ \frac{1}{2}\ \frac{1}{2})_T$ | 0.09 $\mu$B | Neutrons | [118] |

for R = Nd, 5.06 T [106] for R = Ce, and 4.99 T [106] for R = Pr. Averaging for multiple values on the same material and using the conversion that 15 T internal field corresponds to 1 $\mu$B [50, 106], yields an ordered Fe moment to be 0.34 $\mu$B for R = La, 0.35 $\mu$B for R = Nd, 0.34 for R = Ce, and 0.33 for R = Pr. This suggests an ordered Fe moment size which is independent of rare earth ion, as shown in figure 6(a) where the results for R = La, Ce, Pr and Nd are superposed, in apparent contradiction to the neutron results. Zero field $\mu$SR measurements indicate a spontaneous muon spin precession frequency below $T_N$ for all rare earth parent compounds consistent with long range antiferromagnetic order [107]. The size of the magnetic moment is reflected by the saturation frequency which is about 23 MHz for R = La, Pr, Nd, and Sm [103, 107–109, 54]. Interestingly, measurements for R = Ce indicates a significantly higher saturation frequency [107], as can be seen in figure 6(b), suggesting a larger ordered moment consistent with the neutron diffraction measurements and inconsistent with the Mössbauer results. One explanation for this discrepancy is polarization of the Ce sublattice by the ordered Fe moments [107]. Such a polarization would affect the $\mu$SR measurements by modifying the local magnetic field at the muon site and would affect the neutron Bragg reflections under the assumption that the polarized Ce moments exhibit the same periodicity as the ordered Fe moments. The Mössbauer measurements are expected to be less affected as the influence of the Ce moments on the Fe hyperfine field should be small [107].

For the parent compounds with magnetic rare earth ions (i.e. Pr, Ce, Nd, and Sm), the rare earth moments order at low temperatures. The Pr moments in PrFeAsO order below 14 K [99, 101] with a fairly complex ordered structure with Pr spins along the *c*-axis [99]. There is coupling between the Pr and Fe moments and the ordered moments at 5 K were reported to be 0.84 $\mu$B for Pr and 0.48 $\mu$B for Fe [99] (an independent measurement indicated moments at 1.4 K of 0.83 $\mu$B for Pr and 0.53 $\mu$B for Fe [101]). Note that the Fe moment is enhanced from the value of 0.35 $\mu$B observed for temperatures above the Pr ordering temperature [101]. Ce moments in CeFeAsO order below ~4 K with moments lying primarily in the *a*–*b* plane [53]. As in the case of Pr, significant coupling between the Fe and Ce moments is observed with low temperature ordered moments of 0.83 $\mu$B and 0.94 $\mu$B for Ce and Fe respectively which can be compared to the Fe moment of 0.8 $\mu$B at 40 K [53]. Nd spins in NdFeAsO order below 2 K and form a collinear arrangement with antiferromagnetic coupling along the orthorhombic *b* axis [102]. The ordered moments below 2 K were found to be 1.55 $\mu$B for Nd and 0.9 $\mu$B for Fe indicating a strong enhancement when compared to the Fe ordered

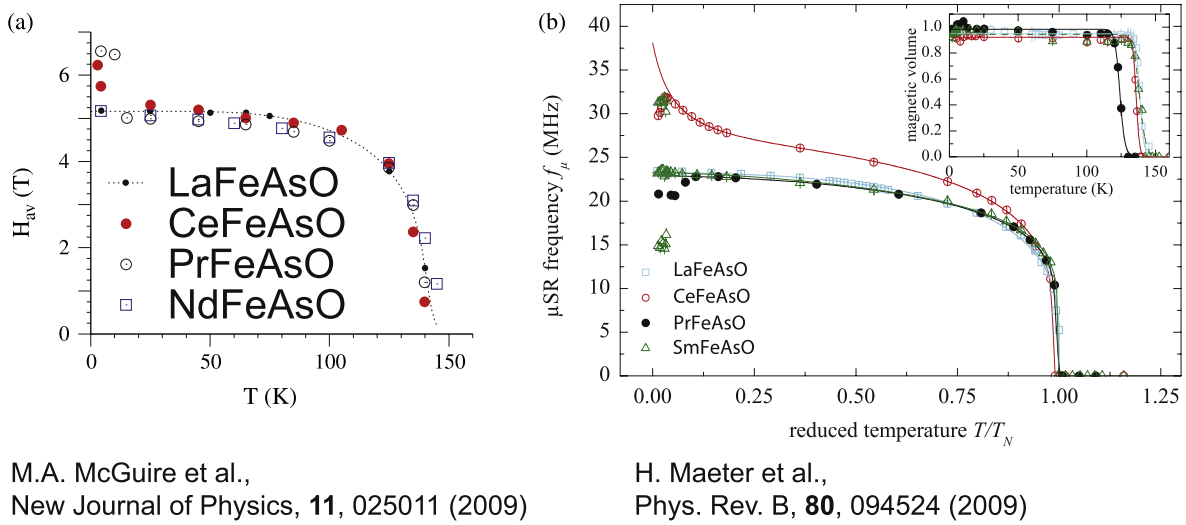


M.A. McGuire et al., New Journal of Physics, **11**, 025011 (2009)

H. Maeter et al., Phys. Rev. B, **80**, 094524 (2009)

**Figure 6.** Measurement of the ordered moment from (a) $^{57}$Fe Mössbauer (reprinted with permission from [106], copyright 2009 IOP Publishing) and (b) $\mu$SR measurements (reprinted with permission from [107], copyright 2009 the American Physical Society). The Mössbauer measurements indicate a moment independent of rare earth element while $\mu$SR measurements show a noticeably different moment for the case of CeFeAsO. Note that the $\mu$SR measurements on CeFeAsO do not appear to saturate at low temperature consistent with a temperature dependent polarization of Ce.

moment of 0.25 $\mu$B observed for temperatures between the Fe and Pr ordering temperatures [98]. Finally, despite the large absorption cross-section of Sm, low temperature measurements on SmFeAsO indicated Sm order at 1.6 K [100]. The determined Sm spin structure is quite different than the other rare earths in that ferromagnetic sheets of Sm moments are stacked antiferromagnetically along the $c$-axis and the ordered Sm moment is 0.6 $\mu$B [100]. In contrast, the cases of Pr, Ce, and Nd have rare earth moments coupled antiferromagnetically along the $b$ axis despite differences in the moment direction [99, 53, 102]. Note that for all measured cases, the Fe ordering arrangement exhibits ferromagnetic coupling along the orthorhombic $b$ axis with an antiferromagnetic arrangement along the $a$-axis.

### *3.2. 122 materials*

The temperature dependent structure of the $AFe_2As_2$ parent compounds has been carefully studied for $BaFe_2As_2$ [59, 60], $SrFe_2As_2$ [84, 114, 113], $CaFe_2As_2$ [120] and $EuFe_2As_2$ [114]. In all cases the room temperature tetragonal space group is $I4/mmm$ and the materials transform to a low temperature orthorhombic $Fmmm$ space group with a 45° rotated cell in the $a$–$b$ plane. The room temperature $I4/mmm$ space group is different than the $P4/nmm$ space group of the 1111 materials in that it contains two FeAs layers per unit cell. In contrast to the 1111 materials, the 122 parent compounds exhibit a structural and magnetic transition at the same temperature as shown in measurements on $BaFe_2As_2$ [60, 110], $SrFe_2As_2$ [111–113, 121], and $CaFe_2As_2$ [115]. Despite some initial contradicting reports, there is now consensus that the magnetic structure is the same in all measured parent compounds. Neutron diffraction measurements on $BaFe_2As_2$ [60, 110, 61], $SrFe_2As_2$ [111, 112], and $CaFe_2As_2$ [115] all indicate a magnetic structure characterized by a $(1\ 0\ 1)_O$ wavevector (where the orthorhombic cell is defined such that $c > a > b$) with moments oriented along the $a$ axis arranged antiferromagnetically along $a$ and ferromagnetically along $b$. Neighboring layers are stacked antiparallel to one another along the $c$-axis. Note that in tetragonal notation, this wavevector corresponds to $(\frac{1}{2}\ \frac{1}{2}\ 1)_T$. The odd-integer value of $L$ in the ordering wavevector is a consequence of the antiferromagnetic stacking along the $c$-axis together with the presence of two layers in a tetragonal unit cell.

Neutron diffraction experiments on the 122 materials find larger ordered magnetic moments than in the 1111 materials which are fairly consistent for different members of the $AFe_2As_2$ family with 0.99 $\mu$B [110] observed in single crystal measurements on $BaFe_2As_2$ (grown with Sn flux), 0.87 $\mu$B [60] in powder measurements on $BaFe_2As_2$, 0.94 $\mu$B in single crystals of $SrFe_2As_2$, 1.01 $\mu$B [112] in powder measurements on $SrFe_2As_2$ and 0.8 $\mu$B in single crystals of $CaFe_2As_2$. This consistency of the ordered moment occurs despite a large variation in transition temperatures ranging from 90 K in $BaFe_2As_2$ grown with Sn flux [110] to 220 K in crystals of $SrFe_2As_2$ [111]. On the other hand, $^{57}$Fe Mössbauer results indicate an internal field of 5.47 T for $BaFe_2As_2$ [108] and much different values of 8.91 T for $SrFe_2As_2$ [114] and 8.5 T for $EuFe_2As_2$ [116]. Interestingly, the Mössbauer internal field shows a similar trend as the magnetic ordering temperature with internal fields of 5.47:8.91:8.5 and transition temperatures of 140:205:200 for Ba:Sr:Eu suggesting that the increased transition temperature is the result of enhanced magnetism in the cases of Sr and Eu. The consistency of magnetic moments from neutron diffraction and inconsistency of the internal fields from Mössbauer measurements in the 122 samples is precisely the opposite of observations on the 1111 materials where the neutron moments were quite different for different rare earths while the Mössbauer fields

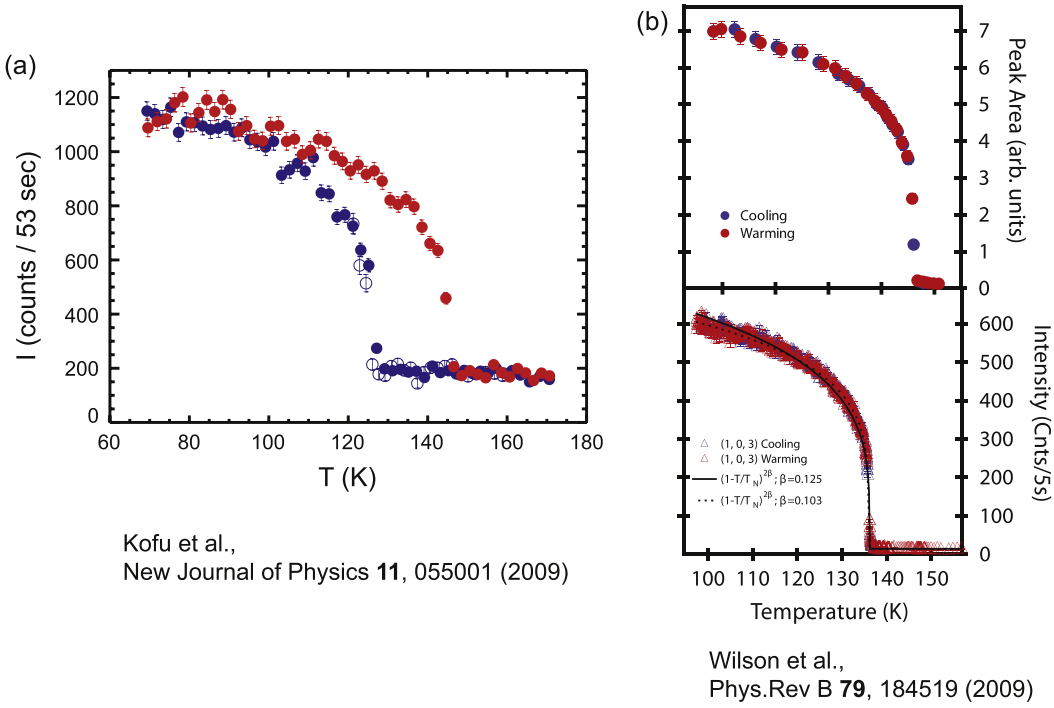


**Figure 7.** Measurements of the Bragg peak intensity on two separate single crystal samples on cooling and warming. The heating/cooling rate in (a) was 2.3 K min$^{-1}$ (solid points) (reprinted with permission from [61], copyright 2009 IOP Publishing) while that in (b) was very slow (<0.05 K min$^{-1}$ average rate) (reprinted with permission from [123], copyright 2009 the American Physical Society). Strong hysteresis is seen in [61] while no hysteresis was observed in [123]. It seems likely that the large difference in hysteresis cannot be fully explained by the rate of temperature change. It has been suggested [123] that difference in sample quality or perhaps external strain due to sample mounting may explain the difference between the hysteresis in various measurements.

were the same. Although the reason for this difference is unclear, it was pointed out that for Mössbauer measurements the proportionality between the hyperfine field and the ordered moment is questionable particularly in light of a potentially unquenched orbital moment [122].

The phase transition in the $AFe_2As_2$ compounds is rather abrupt and the continuous or discontinuous nature of the phase transition in these compounds has been a topic of considerable study. An abrupt change in the order parameter in of itself is not evidence of a first-order transition and may simply be the result of a small critical exponent, $\beta$, in a continuous transition. Hysteresis has been observed in neutron scattering [61, 121, 115], NMR [124, 125] and specific heat measurements [126] suggesting a first-order phase transition. This hysteresis, however, is found to be sample and thermal history dependent. As an example, neutron diffraction measurements on a single crystal $BaFe_2As_2$ sample show a large hysteresis (∼20 K) upon rather rapid warming and cooling (minimum of 2.3 K min$^{-1}$) [61] (as shown in figure 7(a)) while neutron powder diffraction measurements on $BaFe_2As_2$ under conditions of slower warming and cooling (0.25 K min$^{-1}$) shows a smaller hysteresis of less than 10 K [60]. Careful neutron diffraction order parameter measurements also on a single crystal of $BaFe_2As_2$ with a very slow rate of cooling and warming (<0.05 K min$^{-1}$ overall rate) indicate no measurable hysteresis [123] as shown in figure 7(b). The difference in measured hysteresis shown in figure 7 is quite striking and it seems unlikely that such differences can be attributed purely to the rate of temperature change. This suggests that the magnitude of the hysteresis is sample dependent making it difficult to extract the true nature of the phase transition. In addition to hysteresis, further evidence for the first-order nature of the transition was shown in the form of phase coexistence over a finite temperature range observed in neutron diffraction experiments on a single crystal sample of $SrFe_2As_2$ [121].

On the other hand, there is some evidence for a continuous phase transition. We note that the low temperature orthorhombic $Fmmm$ space group is a subgroup of the high temperature tetragonal $I4/mmm$ space group as would be expected for a continuous structural phase transition [114, 59]. Several measurements including neutron diffraction [123] (figure 7(b)) and x-ray diffraction [113] showed no measurable hysteresis. Furthermore, the order parameter can be well parameterized by a power law fit albeit with a very small critical exponent consistent with 2D Ising behavior [114, 123]. It has been suggested [123] that the disparate hysteretic behavior is a consequence of high sensitivity to strain. Such strain may be imposed internally by the inclusion of sample dependent impurities or externally due to the mounting of the crystal and may be sufficient to modify the nature of the phase transition. Indeed, $BaFe_2As_2$ has been known to be quite sensitive to the inclusion of impurities where samples grown in the presence of Sn flux (see, for instance [110]) have a structural/magnetic phase transition at ∼90 K while self-flux grown samples have a very different transition temperature of

~140 K. This difference has been attributed to the inclusion of Sn impurities.

Finally we discuss the evolution of the magnetic structure with doping. Most measurements have focused on $Ba(Fe_{1-x}Co_x)_2As_2$ as the crystals are considered to be homogeneous. Neutron scattering measurements have indicated a magnetic structure characterized by the same $(1\ 0\ 1)_O$ wavevector as the $BaFe_2As_2$ parent compound for concentrations of $x = 0.04$ [67] and $x = 0.047$ [66]. However, NMR measurements on a sample with $x = 0.06$ indicate a distribution of internal fields [76] and $^{57}$Mössbauer measurements on single crystals with $x$ as high as 0.045 indicate a distribution of hyperfine fields [122]. Both observations [76, 122], as well as NMR measurements on other underdoped samples [127], were taken as evidence that the SDW order evolves from commensurate for the parent compound to incommensurate in the presence of Co doping. Modeling the NMR lineshape yields the prediction of a small incommensuration with magnitude $\varepsilon \sim 0.04$ [76]. The particular case considered involved a $(1-\varepsilon, 0, L)_O$ wavevector [76]. We note that for the neutron measurements reported [66, 67] the resolution at the orthorhombic (1 0 1) wavevector is less than 0.02 r.l.u. along $h$ which would have easily allowed for measurements of an incommensuration of the value estimated above. However, an incommensuration significantly smaller than this resolution is certainly possible. Furthermore, the resolution along the orthorhombic $k$ direction (the vertical direction experimentally) is very coarse and an incommensuration along this direction would be difficult to detect in these experiments. High resolution neutron diffraction experiments are needed to resolve this issue.

### *3.3. 11 materials*

The structural and magnetic properties of the 11 family of compounds is complicated by extreme sensitivity to stoichiometry and the presence of excess Fe. As an example, nearly stoichiometric $FeSe_{0.97}$ crystallizes in the $P4/nmm$ tetragonal space group while a small variation in concentration to $FeSe_{1.06}$ induces a phase change and the material exhibits a hexagonal structure [128]. Furthermore, superconductivity in $Fe_{1.01}Se$ with $T_C \sim 8$ K is destroyed by increasing the amount of excess Fe and no superconductivity is observed down to 0.6 K in samples of $Fe_{1.03}Se$ [129]. The phase of interest with respect to superconductivity is the $\alpha$ phase (curiously this phase is occasionally referred to in the literature as the $\beta$ phase). Magnetic ordering is observed in samples close to the Te endpoint member of the $Fe_{1+y}Te_{1-x}Se_x$ family. Structurally, $Fe_{1+y}Te$ exhibits the PbO crystal structure with a space group of $P4/nmm$ at room temperature for values of $y$ ranging from 0.068 to 0.14 [44, 117]. At low temperatures, a first-order structural transition is observed (transition temperature ~65 K [130]) and the low temperature space group is the monoclinic $P2_1/m$ for samples of $Fe_{1.076}Te$ [44] and $Fe_{1.068}Te$ [117]. On the other hand, a small change in $x$ to $Fe_{1.141}Te$ changes the low temperature unit cell to orthorhombic with the $Pmmn$ space group [44] again providing evidence for sensitivity to stoichiometry. In both the orthorhombic and monoclinic unit cells, there is no cell doubling or cell rotation when compared to the tetragonal cell and, hence, the Miller indices of Bragg reflections are the same for all unit cells [44].

The magnetic structure and low temperature monoclinic distortion of $Fe_{1.125}Te$ was first determined 35 years ago [131]. The magnetic structure was characterized by an ordering wavevector of $(\frac{1}{2}\ 0\ \frac{1}{2})$ with a rather large ordered magnetic moment of 2.07 $\mu$B with components of magnetic moment along all crystallographic axes [131]. Recent neutron diffraction measurements indicate ordering with the same commensurate $(\frac{1}{2}\ 0\ \frac{1}{2})$ wavevector in the case of $Fe_{1.075}Te$ [44] and $Fe_{1.068}Te$ [117] where the low temperature structure is monoclinic. The data are consistent with a collinear spin structure [131, 44, 117], as shown in figure 5(b). The more recent studies indicated an ordered moment of 2.03 $\mu$B for $x = 0.075$ [44] and 2.25 $\mu$B for $x = 0.068$ [117] with the majority of the moment along the crystallographic $b$-axis [44, 117]. (Note that the moment direction is different than the earlier magnetic structure determination [131].) Interestingly, the samples which exhibit a low temperature orthorhombic structure are found to order magnetically with an incommensurate wavevector of $(\pm\delta, 0, \frac{1}{2})$ with $\delta \approx 0.38$ [44]. The addition of Se causes the long range magnetically ordered state to evolve into short range order centered at incommensurate wavevectors $(0.5 - \delta\ 0\ 0.5)$ [44, 132]. Single crystal studies of two samples, $Fe_{1.07}Te_{0.75}Se_{0.25}$ and $FeTe_{0.7}Se_{0.3}$ indicate that less excess Fe and more Se makes the incommensuration smaller, such that the scattering is closer to (0.5 0 0.5), and the intensity weaker as well [132]. Interestingly, peaks are only observed on one side of the 2D (0.5 0) wavevector (i.e. the wavevector is $(0.5 - \delta, 0, 0.5)$ and not $(0.5 \pm \delta, 0, 0.5)$) although the observed incommensuration is reproduced with a model of exponentially decaying correlations where the characteristic length scale of the exponential is different for ferromagnetic and antiferromagnetic correlations [132].

The wavevector observed in the 11 materials is different than that observed in the 1111 or 122 materials with an in-plane wavevector of $(\frac{1}{2}\ 0)_T$ as opposed to $(\frac{1}{2}\ \frac{1}{2})_T$ seen in both the 1111 and 122 compounds. Interestingly, this happens despite calculated Fermi surfaces that are very similar suggesting that the 11 materials should be susceptible to a nesting instability with the same $(\frac{1}{2}\ \frac{1}{2})_T$ nesting wavevector [43]. Calculations indicate that excess Fe in these materials is magnetic [45], consistent with the conclusions of neutron structure refinements [44]. However, these calculations indicate that the lowest energy ground state is still the $(\frac{1}{2}\ \frac{1}{2})_T$ state [45] even in the presence of excess Fe. It was further proposed that the excess Fe could cause a mismatch in size between the $\Gamma$ and M parts of the Fermi surface which could lead to incommensurate magnetism [133]. Experimentally, ARPES measurements confirmed the calculated Fermi surface and further showed that the $\Gamma$ and M parts of the Fermi surface are closely matched [134]. In addition, despite a weak feature at the X point, these measurements seem to rule out Fermi surface nesting along the observed $(\frac{1}{2}\ 0)_T$ wavevector. As Fermi

surface nesting seems very unlikely in this case, theoretical approaches to understand the ordering have focused on local moment models. First-principles calculations have predicted bicollinear order due to the presence of near-neighbor, next-near-neighbor and next-next-near-neighbor interactions [135]. This model was expanded upon and the phase space of the various exchange constants was explored indicating not only ordering with the commensurate $(\frac{1}{2}\ 0)_{\mathrm{T}}$ wavevector but also incommensurate ordering [136] as observed experimentally with higher amounts of excess Fe [44]. It was also suggested that interaction of the FeTe spins with the magnetic excess Fe moments could modify the superexchange interactions leading to the incommensuration observed experimentally [136]. One alternate model, described previously, results in local moments but with magnetic interactions which are long-ranged itinerant interactions and not superexchange [96]. These DFT calculations, when applied to FeTe, indicate that the $(\frac{1}{2}\ 0)_{\mathrm{T}}$ ordering and $(\frac{1}{2}\ \frac{1}{2})_{\mathrm{T}}$ ordering were energetically very similar as opposed to the 122 case where the $(\frac{1}{2}\ \frac{1}{2})_{\mathrm{T}}$ ground state was clearly favored [96].

## 4. Spin dynamics

A comprehensive understanding of the relationship between magnetism and superconductivity in the Fe-based superconductors ultimately requires understanding not only the nearby magnetic ground states, but the full magnetic excitation spectrum. Indeed, once the close proximity of a magnetic state in the phase diagram was discovered theories postulating a magnetic pairing mechanism were quickly put forth (e.g. see [137–140]). Concurrently, the importance of spin fluctuations was established from an experimental point of view where early studies of the spin dynamics [141–145] revealed the presence of strong magnetic fluctuations in the superconducting region of the phase diagram. Thus, a key step in confirming or rejecting theories of superconductivity relying on a magnetic pairing mechanism requires the elucidation of the magnetic excitation spectrum and thereby an effective Hamiltonian.

In this section the spin dynamics are discussed as revealed primarily by inelastic neutron scattering (INS) and in some cases supplemented by NMR measurements. Note that the two probes are complementary: the NMR energy window is substantially less than INS experiments where energy resolutions are not typically better than 0.1 meV. On the other hand, INS experiments can probe excitations to as high as 300 meV and beyond. In section 4.1 the spin dynamics found in the parent compounds are discussed. Section 4.2 discusses the evolution of the spin dynamics with chemical doping, pressure, and magnetic field. Finally, section 4.3 is reserved for a comprehensive discussion of the magnetic resonance at various chemical compositions and magnetic fields.

### *4.1. Spin dynamics in the parent compounds*

The present understanding of the spin dynamics in the parent compounds is still evolving. However, many characteristics of the spin excitations are already well established. Below $T_{\mathrm{N}}$, the spin excitations are characterized by gapped steeply dispersing anisotropic three-dimensional (3D) spin waves extending to high energies. Above $T_{\mathrm{N}}$ the spin excitations appear to lose much of their 3D character with correlations along the $c$-axis considerably weakened while the in-plane correlations remain strong. Because of the large energy scale of both the spin excitations and the gap values most of the current understanding of the spin excitations is derived from analysis of INS data. Many INS experiments have been performed at energies small compared to the zone boundary energy. In this limit, what is experimentally observed are spin excitations which can be characterized by an antiferromagnetic zone center energy gap and spin wave velocities most commonly along two directions as the majority of experiments performed to date have used a triple-axis spectrometer where measurements are performed in a fixed plane. In order to attempt to extract interaction energies from these velocities, a local moment Heisenberg Hamiltonian has often been adopted. As the nature of the magnetic interactions (i.e. local versus itinerant) is still the topic of considerable debate, such a mapping should be taken *cum grano salis*. For the 122 materials, the Hamiltonian most widely used is [146, 147]:

$$H = \sum_{\langle jk \rangle} (J_{jk} S_j \cdot S_k) + \sum_j \{D(S_z^2)_j\} \tag{1}$$

where $J_{jk}$ are exchange constants and $D$ represents a single ion anisotropy term, included to describe the observed energy gap. The magnetic excitations can be described using three in-plane exchange constants; the near-neighbor interactions $J_{1a}$ and $J_{1b}$ (different due to the orthorhombic distortion) and the next-near-neighbor interaction $J_2$ as shown in figure 8. There is also a single $c$-axis nearest neighbor exchange constant $J_c$. This Hamiltonian results in the following spin wave dispersion

$$\omega_q = \sqrt{A_q^2 - B_q^2} \tag{2}$$

where

$$\begin{aligned} A_q &= 2S(J_{1b}(\cos \pi K - 1) + J_{1a} + 2J_2 + J_{1c} + D) \\ B_q &= 2S(J_{1a} \cos \pi H + 2J_2 \cos \pi H \cos \pi K + J_{1c} \cos \pi L). \end{aligned} \tag{3}$$

In the above expressions, $H, K, L$ are the reciprocal space coordinates corresponding to the orthorhombic unit cell. The majority of the triple-axis experiments have been performed in the $(H0L)_{\mathrm{O}}$ scattering plane. In this plane, the spin wave velocities [148] and energy gap are:

$$\begin{aligned} v_{\parallel} &= aS(J_{1a} + 2J_2)\sqrt{1 + J_{1c}/(J_{1a} + 2J_2)} \\ v_{\perp} &= cSJ_{1c}\sqrt{1 + (J_{1a} + 2J_2)/J_{1c}} \\ \Delta &= \sqrt{D(D + 2(J_{1a} + 2J_2 + J_{1c}))}. \end{aligned} \tag{4}$$

Note that these observables are insensitive to the value of $J_{1b}$ and only depend on the in-plane interactions as $J_{1a}$–$2J_2$. Determination of $J_{1b}$ or the unique determination of $J_{1a}$ and $J_2$ requires measurements not restricted to a plane and extending to higher energies as can be obtained from time-of-flight data [149, 150].

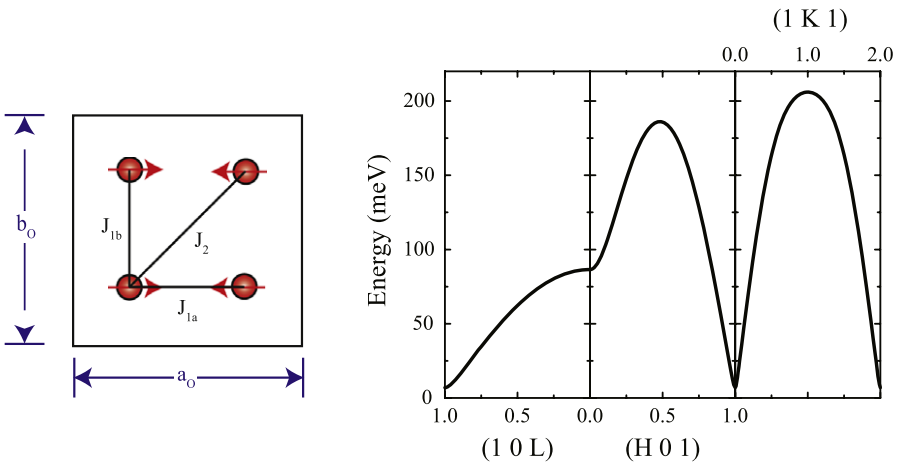


**Figure 8.** (a) Exchange constants for the Heisenberg model given in the text. Note that $J_c$ (not shown) is the nearest neighbor interaction to the Fe ion directly above. (b) Dispersion of $CaFe_2As_2$ calculated with the parameters from [150]. Note the change in index going from the $(H01)_O$ direction to the $(1K1)_O$ direction.

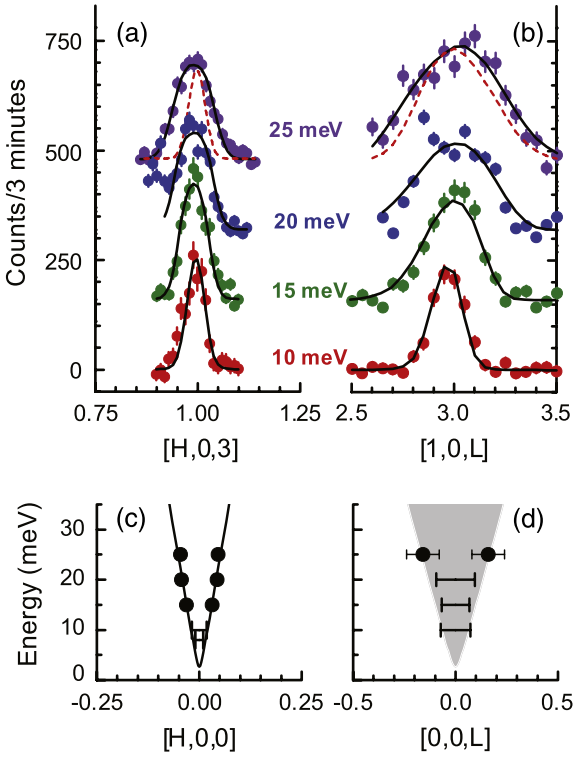


**Figure 9.** Representative INS scans on $CaFe_2As_2$ in the long-wavelength limit (reprinted with permission from [148], copyright 2008 the American Physical Society). Constant energy scans are shown along (a) $(H\ 0\ 3)_O$ and (b) $(1\ 0\ L)_O$. The resulting dispersion is shown in (c) and (d) showing the 3D anisotropic spin waves.

For completeness, we note that INS experiments measure $S(\mathbf{Q}, \omega)$ which is related to the imaginary part of the dynamic susceptibility, $\chi''(\mathbf{Q}, \omega)$, by

$$S(\mathbf{Q}, \omega) = \frac{\chi''(\mathbf{Q}, \omega)}{\pi(1 - e^{-\hbar\omega/k_B T})}. \quad (5)$$

We now turn to a discussion of the spin waves in the magnetically ordered state in the 122 family of materials. The spin excitation spectrum has been measured using INS on samples of $BaFe_2As_2$ [146, 151], $CaFe_2As_2$ [148–150, 152], and $SrFe_2As_2$ [153]. Figure 9 shows representative scans taken from INS measurements of the spin excitations in an array of $CaFe_2As_2$ single crystals [148]. Visual inspection of this data allows for the qualitative understanding of some generic properties of the 122 materials. In particular, significant dispersion is visible along both the $H$ and $L$ directions. Hence, the interactions can be characterized as anisotropic 3D interactions, in contrast to the 2D magnetic interactions found in the cuprates [154]. Moreover, it is clear that the spin excitations are steeply dispersive, with an early study by Ewings *et al* estimating a bandwidth of 170 meV [146] suggesting strong magnetic interactions, as in the cuprates.

Table 3 presents a summary of the coupling constants $S(J_{1a} + 2J_2)$, $SJ_c$, energy gap, and spin wave velocities extracted from INS on 122 parent compounds (together with the underdoped sample $BaFe_{1.92}Co_{0.08}As_2$ [67]). The ratio of spin wave velocities $(v_\parallel/v_\perp)$ is a measure of the anisotropy of the magnetic excitations with an infinite ratio observed for purely in-plane (2D) excitations and unity for isotropic 3D interactions. As can be seen in table 3 the spin wave velocity ratio varies from 1.5 to 5. Anisotropy in the low energy spin fluctuations is also concluded from NMR data [124, 125] with $BaFe_2As_2$ being more anisotropic than $SrFe_2As_2$, a trend that is reflected in table 3. Interestingly, the spin wave velocity ratio in $BaFe_2As_2$ is notably higher than the Ca and Sr parent compounds indicating more 2D interactions in this material and it is also the Ba-122 compounds that exhibit the highest superconducting transition temperatures for the same dopant (see table 1). This may suggest that 2D interactions are favorable for superconductivity.

Another prominent feature of the spin wave data in the parent compounds is the presence of a gap in the excitation spectrum (see table 3 for the gap extracted from INS measurements). The opening of a gap in the spin excitation spectrum is also reflected in the temperature dependence of the NMR data (e.g. [155]). The gap largely disappears above $T_N$ [153, 152] while well below $T_N$ the gap appears to be rather

**Table 3.** Exchange constants extracted from inelastic neutron scattering on 122 single crystals using an effective Heisenberg Hamiltonian. All energies are reported in units of meV and spin wave velocities in units of meV Å. The value of the energy gap is lineshape dependent and thus care should be taken when making comparisons between studies.

| Material | $S(J_{1a}+2J_2)$ | $S(J_c)$ | Energy gap | $v_\parallel$ | $v_\perp$ | $v_\parallel/v_\perp$ |
|---|---|---|---|---|---|---|
| $CaFe_2As_2$ [148] | $73 \pm 14$ | $6.7 \pm 3$ | $6.9 \pm 0.2$ | $420 \pm 70$ | $270 \pm 100$ | 1.56 |
| $CaFe_2As_2$ [150] | $87.7 \pm 12$ | $5.3 \pm 1.3$ | — | $498 \pm 70$ | $259 \pm 116$ | 1.92 |
| $CaFe_2As_2$ [149] | $91.5 \pm 1.2$ | $4.5 \pm 0.1$ | — | $516 \pm 7$ | $243 \pm 7$ | 2.12 |
| $SrFe_2As_2$ [153] | $100 \pm 20$ | $5 \pm 1$ | 6.5 | $560 \pm 100$ | $280 \pm 56$ | 2 |
| $BaFe_2As_2$ [151] | $50 \pm 27$ | $0.38 \pm 0.15$ | $9.8 \pm 0.4$ | $280 \pm 150$ | $57 \pm 7$ | 4.91 |
| $BaFe_{1.92}Co_{0.08}As_2$ [67] | $32 \pm 1$ | $0.34 \pm 0.01$ | $8.1 \pm 0.2$ | $180 \pm 12$ | $43 \pm 2$ | 4.19 |

broad [146, 151]. Ewings *et al* put forth idea that multiple gaps may exist that experimental resolution is insufficient to resolve. While a single ion anisotropy is included in the effective Heisenberg Hamiltonian used to extract the gap, this is really ad hoc and, thus, an unresolved question is the nature and origin of the gap in the spin wave spectrum.

As mentioned above, unique determination of $J_{1a}$, $J_{1b}$ and $J_2$ require measurements not restricted to a single scattering plane and extending to the zone boundary. Such measurements using time-of-flight INS were performed on single crystals of $CaFe_2As_2$ resulting in effective nearest neighbor exchange interactions of $SJ_{1a} \sim 50(10)$ meV, $SJ_{1b} \sim -6(5)$ meV and a rather large next nearest exchange interaction of $SJ_2$ of 19(3) meV [150]. The dispersion (equations (2) and (3)) calculated from these parameters is shown in figure 8. The observation of antiferromagnetic $J_{1a}$ and $J_2$ and ferromagnetic $J_{1b}$ shows that, unlike theoretical predictions [92–94], the magnetic interactions are not frustrated. However, the relatively large size of $J_2$ is consistent with theory [92–94] and the measured ratio of $J_{1a}/2J_2$ is $\sim$1.3(3). The anisotropy in the nearest neighbor exchange constants is striking for a system that is tetragonal at room temperature. Similar anisotropy was predicted from a combination of DFT calculations and linear response theory suggesting rather short range interactions and exchange constants close to experimental observation (for instance, the calculated $J_{1a}/2J_2$ ratio is $\sim$1 for various FeAs parent compounds) [156]. An alternative model was proposed which involves breaking the in-plane rotational symmetry via orbital ordering suggesting that orbital degrees of freedom may play an important role in these materials [97]. Further experimental work, particularly with full control over all three reciprocal space coordinates is crucial in this area.

The experimental situation in the parent compound in other families of materials is much less settled, primarily do the lack of large single crystals. To our knowledge, there have only been two investigations of the spin excitations in the 1111 family of materials. Despite the limitations of polycrystalline samples and the resulting spherical averaging of the spin excitation spectrum, the studies showed a spectrum qualitatively similar to that observed in the 122 parent compounds. Measurements on LaFeAsO [157] revealed a column of spin wave excitations emanating from a wavevector consistent with $(10L)_O$. Well above the magnetic ordering temperature the peak shape exhibits an asymmetry in Q interpreted as being consistent with two-dimensional (2D) spin fluctuations. Given this as well as the fact that the excitations are steeply dispersing, these measurements are consistent with strong in-plane exchange interactions between Fe atoms [157]. Further work on the Fe-spin excitations in the other 1111 has been hampered by the overlap with crystal field excitations of the rare earth ions. The crystal field excitations in the 1111 materials have been explored for the case of $CeFeAsO_{1-x}F_x$ [158]. In the disordered state, the observed crystal field excitations are consistent with the expected system of three doublets for $Ce^{3+}$ in a tetragonal environment [158]. Below the Fe magnetic ordering temperature, the degeneracy of the doublets is lifted due to the internal field of the magnetically ordered Fe sublattice. Finally, in the 11 family, limited data exists with measurements on a polycrystalline sample of $FeTe_{0.92}$ [159] indicating spin excitations at a Q consistent with the magnetic ordering (0.5 0 0.5) wavevector [44].

In principal, the study of the spin excitations can provide information concerning whether or not the spin degrees of freedom are derived from localized or itinerant electrons. In an itinerant antiferromagnet, there should be significant damping due to decay of the spin waves into electron–hole pairs. Measurements on $CaFe_2As_2$ [148] and $BaFe_2As_2$ [151] suggested that considerable damping is present in the spin wave spectrum as expected for an itinerant system. On the other hand, measurements of the full excitation spectrum in $CaFe_2As_2$ are well described by a Heisenberg Hamiltonian [150] with some damping ($\Gamma \sim$ 0.15 E) which they attribute to predominately local moment physics. Interestingly, despite the contradictory conclusions with respect to itinerancy, the magnitude of damping extracted by McQueeney *et al* [148] and Zhao *et al* [150] both on $CaFe_2As_2$ are largely consistent with one another. Ultimately there may well be aspects of both localized and itinerant magnetism as predicted from DFT calculations where it was suggested that the moments were local but the interactions were itinerant in nature [96].

### *4.2. Evolution of the spin excitations*

We now turn to the evolution of the spin excitations as a function of a tuning parameter. Much of the experimental effort so far has been directed towards understanding the spin resonance which appears in the spin excitation spectrum below $T_C$ which will be discussed in detail in section 4.3. Here we concentrate on the more general evolution of the spin excitations. In fact, the normal state spin excitations, assuming

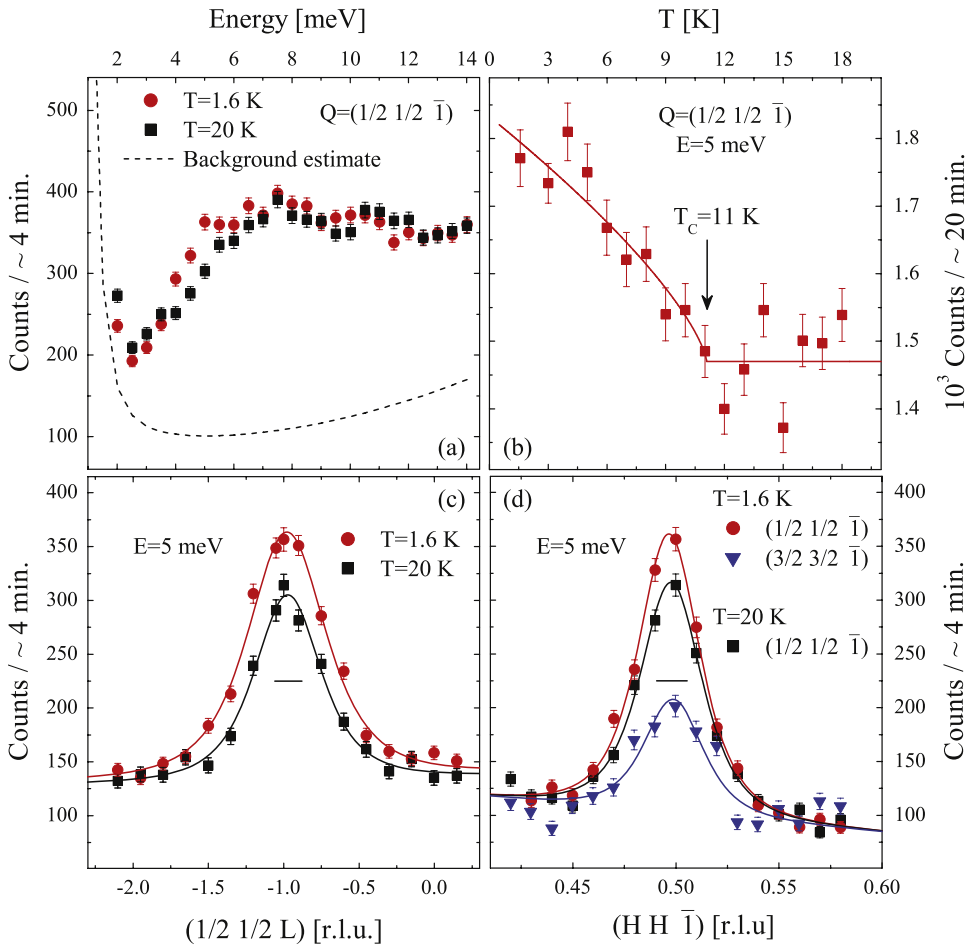


**Figure 10.** INS data for underdoped $BaFe_{1.92}Co_{0.08}As_2$ (Reprinted with permission from [67], copyright 2009 the American Physical Society). (a) Constant-**Q** scans, $\mathbf{Q} = (\frac{1}{2}\ \frac{1}{2}\ -1)_T$, for temperatures above and below $T_C$ together with the estimated background. (b) The temperature dependence of the inelastic intensity at $(\frac{1}{2}\ \frac{1}{2}\ -1)_T$ and $E = 5$ meV. The solid line is a power law fit yielding $T_C = 11(1)$ K. $L$-dependence (c) and $H$-dependence (d) of the inelastic intensity near $\mathbf{Q} = (\frac{1}{2}\ \frac{1}{2}\ -1)_T$ and $E = 5$ meV at 1.6 and 20 K. The solid lines are guides to the eye and horizontal bars represent instrumental resolution. In (d) a scan around $(\frac{3}{2}\ \frac{3}{2}\ -1)_T$ is included to emphasize the magnetic origin of the scattering.

a magnetically mediated pairing mechanism, must contain the necessary spectral weight to facilitate pairing. The most common tuning parameter to date has been chemical doping, though applied magnetic fields and pressures have also been used. In this section we will largely limit discussion to three main classes of materials ($Ba(Fe, Co, Ni)_2As_2$, LaFeAs(O, F), and Fe(Te, Se)) as they exemplify the characteristic behavior of the Fe-based materials.

The spin dynamics in the $Ba(Fe_{1-x}Co_x)_2As_2$ has been studied by several groups [144, 66, 67, 160–162]. In the underdoped region, the spin excitations of a single crystal sample of magnetically ordered ($T_N = 58$ K) and superconducting ($T_C = 11$ K) $BaFe_{1.92}Co_{0.08}As_2$ were studied in the long-wavelength limit [67]. In accord with the results in $BaFe_2As_2$ the excitations are peaked in both $H$ and $L$ so it is clear that the magnetic interactions, though anisotropic, are 3D (see figure 10). The anisotropy of the magnetic interactions as characterized by the ratio of the $v_\parallel/v_\perp$ is about 4.2 consistent with the value found in the $BaFe_2As_2$ [151]. The low temperature spin waves are characterized by a gap ($\Delta \sim$ 8 meV), comparable to that found in the parent compound $BaFe_2As_2$ [151]. Note, however, that care must be taken when making such comparisons as the gap energy is lineshape dependent.

Optimally doped $BaFe_2As_2$ has been studied for the case of Co and Ni doping. As discussed earlier, in the optimally doped region of the phase diagram long range magnetic order has been suppressed (see figure 2). Initial studies of $BaFe_{1.84}Co_{0.16}As_2$ ($T_C = 22$ K) with INS showed a striking reduction of the spin correlations along the $c$-axis as shown by a visual inspection of in-plane and $c$-axis scans [144]. The ratio of the in-plane to $c$-axis bandwidths allows a more quantitative determination of the degree of two-dimensionality. To that end, data on $BaFe_{1.84}Co_{0.16}As_2$ was analyzed with a dispersion composed of a gap with in-plane and $c$-axis coupling constants. From this model an estimate of the ratio of in-plane to $c$-axis bandwidths of 117 (with a lower limit of 40) was determined. This ratio is much larger than that of the parent compounds (see figure 8 for $CaFe_2As_2$ and the spin wave velocity ratio of table 3). This confirms a substantial reduction in $c$-axis

correlations relative to those in the tetragonal plane. Thus, the dimensionality of the magnetic interactions has shifted from anisotropic 3D in the parent compounds towards 2D. Although INS measurements on optimally doped $Ba_{1.9}Ni_{0.1}As_2$ ($T_C$ = 20 K) are primarily focused on elucidating the behavior of the spin resonance, they also observe a reduction in the magnetic correlations along the $c$-axis [145]. This reduction is apparently not as large as for the case of $Ba_{1.84}Co_{0.16}As_2$, but a more quantitative analysis of both the in-plane and $c$-axis dispersion is required before a firm comparison can be made. The spin excitations of $Ba_{1.84}Co_{0.16}As_2$ with $T_C = 25$ K were followed to high temperatures and up to 35 meV [160] and the resulting spectrum analyzed with a model for a nearly antiferromagnetic Fermi liquid [163]. The data were normalized to be in absolute units and that they were able to extract a total spectral weight in the normal state spin fluctuations of 0.17 $\mu_B^2$/f.u. up to 35 meV [160]. This value is comparable to that found for underdoped $YBa_2Cu_3O_{6+x}$ [164].

There have been somewhat fewer studies of the spin dynamics in the 122 materials in the overdoped region. NMR investigations have probed the evolution of the spin excitations into the overdoped region in $Ba(Fe_{1-x}Co_x)_2As_2$ [165]. These measurements find that as $T_C$ is suppressed by Co doping so are the low energy spin fluctuations. Higher energy spin excitations in the $Ba(Fe_{1-x}Co_x)_2As_2$ series have been studied with INS into the overdoped region [161]. In this region two concentrations, $x = 0.14$ ($T_C = 7$ K) and $x = 0.24$ ($T_C = 0$) are studied. For $x = 0.14$ intensity is observed at $(1\ 0\ 1)_O$ that appears to be consistent with gapped spin excitations, at 10, 30 and 100 K, which is substantially different from the more lightly doped samples where a gap in the spin excitations does not appear until the onset of long range magnetic order or superconductivity. The observation of gapped spin excitations may also explain the disappearance of spin fluctuations at $x > 0.15$ seen with NMR [165] as such a gap would effectively redistribute the spectral weight outside the NMR measurement window. Matan, *et al* also examined a sample where superconductivity has been fully suppressed by doping and were unable to observe spin fluctuations [161]. They argue that this observation is further evidence that the magnetic excitations are due to nesting between the hole and electron Fermi surfaces as the hole pocket should have effectively disappeared at this concentration [166]. On the other hand, recent NMR studies of hole doped $Ba_{1-x}K_xFe_2As_2$ [167] are consistent with the development of a new type of spin fluctuation developing near $KFe_2As_2$ perhaps suggesting a different pairing symmetry on the overdoped side of the phase diagram [167].

The available studies of the $LaFeAsO_{1-x}F_x$ series are also consistent with the disappearance of spin fluctuations as the hole pocket is filled by electron doping. The low energy spin fluctuations in polycrystalline samples of $LaFeAsO_{1-x}F_x$ were explored with INS [168]. They find similar spin excitations to those found in LaFeAsO [157]. However, in the overdoped region, the spin fluctuations are observed to have nearly vanished in accord with a close relationship between spin fluctuations and superconductivity. Thus, in at least two cases (Ba122 and La1111) when antiferromagnetically ordered parent compounds are overdoped by electron doping the spin fluctuations vanish as the hole pocket vanishes.

$CaFe_2As_2$ provides an interesting case to study the evolution of the spin excitations as a function of pressure. Initially, it was thought that $CaFe_2As_2$ exhibited pressure induced superconductivity at relatively low pressures [169, 170]. More recent studies under hydrostatic pressure do not support bulk superconductivity in the high pressure state [171]. Given this, the neutron scattering studies as a function of pressure [172] show that in the pressure region of the collapsed tetragonal phase where long range magnetic order has been suppressed [173] the spin fluctuations are also absent. This is in contrast to chemical doping in the 122 materials where strong spin fluctuations are observed despite the suppression of long range magnetic order. In this case, superconductivity is not supported in the absence of spin fluctuations.

The spin excitations in $FeTe_{1-x}Se_x$ have been studied by a number of groups [174, 159, 175–179]. The majority of the investigations of the spin excitations in $FeTe_{1-x}Se_x$ have focused on investigation of the magnetic resonance feature which will be discussed in greater detail in section 4.3. An interesting early development in the study of the spin excitations was that, in contrast to the parent compound where the magnetic order occurs near $(0.5\ 0\ 0.5)_T$, the spin fluctuations in superconducting samples were found to be near $(0.5\ 0.5\ 0)_T$ [174, 159, 175] (see figure 5). Thus, the spin correlations in the plane were at a similar wavevector as found in the other Fe-based materials perhaps hinting at the fact that spin fluctuations of a certain type are needed for superconductivity in the Fe-based materials.

Lumsden, *et al* followed the spin excitations up to 250 meV in single crystal samples [176] (see figure 11). A superconducting sample with a $T_C$ of 14 K ($FeTe_{0.51}Se_{0.49}$) as well as a sample which did not exhibit bulk superconductivity ($Fe_{1.04}Te_{0.73}Se_{0.27}$) were measured with INS enabling comparisons of the spin excitations for the two cases. Both samples showed spin excitations which were 2D in character consistent with measurements over a more limited energy range in $FeTe_{0.6}Se_{0.4}$ [175]. The observed excitations originate from a wavevector near $(0.5\ 0.5\ 0)_T$ but the zero energy extrapolation of the dispersion indicates that the excitations are incommensurate forming a low energy quartet of peaks characterized by the wavevectors $(1 \pm \xi, \pm\xi, L)_T$ and $(1 \pm \xi, \mp\xi, L)_T$ [176]. The observed periodicity of the spin excitations is consistent with the 2D square lattice of Fe atoms indicating that this unit cell contains the necessary information to describe the magnetism. Triple-axis measurements have been performed on a sample of $FeTe_{0.6}Se_{0.4}$ confirming the incommensurate nature of the spin excitations [177]. More recently, several observations have appeared that suggest that the symmetry of the spin excitations observed in the $FeTe_{1-x}Se_x$ system is common to the 122 materials as well. In optimally doped $Ba(Fe, Co)_2As_2$ two groups have observed a discrete set of spots with an in-plane anisotropy similar to that observed in $FeTe_{1-x}Se_x$ rather than a cone as might be expected for a conventional spin wave [162, 180]. Similar observations appear to hold for the spin excitations in the paramagnetic state of $CaFe_2As_2$ [152] where a smaller

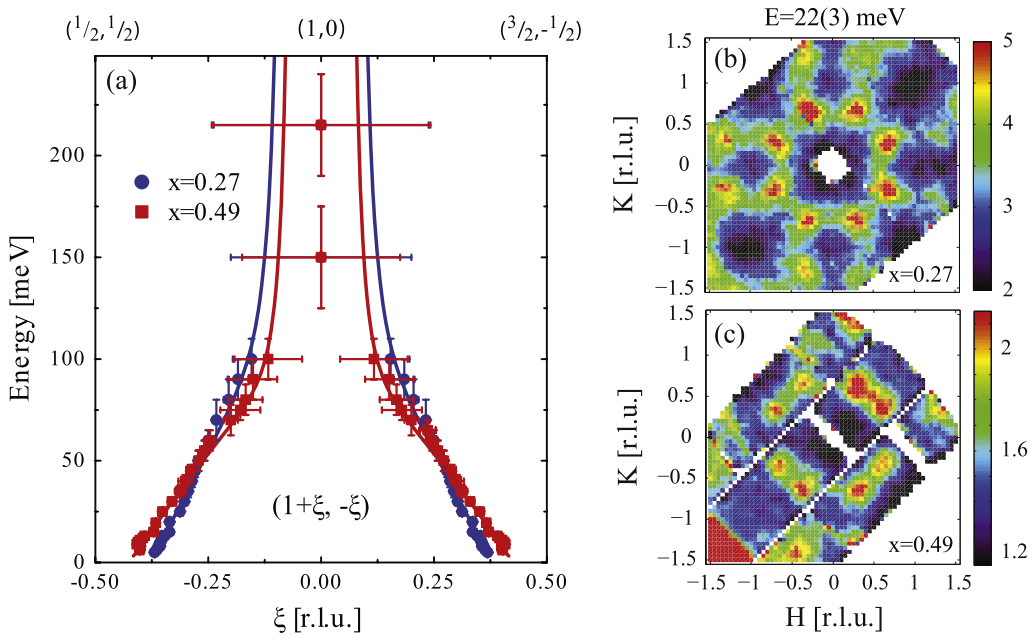


**Figure 11.** Spin excitations in $FeTe_{1-x}Se_x$ (reprinted by permission from Macmillan Publishers Ltd: Nature Physics [176], copyright 2010). (a) Dispersion of the spin excitations for $x = 0.27$ (0.49) blue circles (red squares). (b) and (c) are constant energy slices of the scattering projected onto the 2D $(H\ K)_T$ plane for $x = 0.27$ (b) and for $x = (0.49)$ (c).

**Table 4.** Comparison of spin resonance energies in various Fe-based materials. The references for the experimental determination of the superconducting gap are also given, where available, in the reference column. The heavy fermion superconductor $CeCoIn_5$ is included for comparison.

| Material | $T_C$ (K) | $E_r$ (meV) | $E_r$ ($k_BT_C$) | $E_r/2\Delta_{max}$ | Reference |
|---|---|---|---|---|---|
| $Ba_{0.6}K_{0.4}Fe_2As_2$ | 38 | 14 | 4.3 | 0.58 | [143, 201] |
| $LaFeAsO_{0.918}F_{0.082}$ | 29 | 12.9(1) | 5.2 | — | [197] |
| $BaFe_{1.85}Co_{0.15}As_2$ | 25 | 9.5 | 4.4 | 0.79 | [160, 200, 202, 203] |
| $BaFe_{1.84}Co_{0.16}As_2$ | 22 | 8.6(5) | 4.5 | 0.69 | [144, 203] |
| $BaFe_{1.9}Ni_{0.1}As_2$ | 20 | 7.0(5)–9.1(4) | ∼4.7 | — | [145, 121] |
| $FeTe_{0.5}Se_{0.5}$ | 14 | 6–7 | ∼5.4 | — | [174, 178] |
| $FeTe_{0.5}Se_{0.5}$ | 14 | 6–6.5 | ∼5.2 | — | [179, 196] |
| $FeTe_{0.6}Se_{0.4}$ | 14 | 6.51(4) | 5.4 | — | [175, 177] |
| $BaFe_{1.92}Co_{0.08}As_2$ | 11 | 4.5(5) | 4.7 | — | [67] |
| $CeCoIn_5$ | 2.3 | 0.60(3) | 3.0 | 0.65 | [193] |

anisotropy of the spin excitations around the $(0.5\ 0.5\ L)_T$ has been observed.

The observation of a quartet of low energy incommensurate inelastic peaks characterized by the square lattice wavevectors $(\pi \pm \xi, \pi)$ and $(\pi, \pi \pm \xi)$ is intriguing since the low energy excitations in the cuprates show very similar behavior [181]. This indicates strong similarities in the excitation spectrum of Fe- and Cu-based superconductors which, under the assumption of magnetically mediated superconductivity, may suggest a common origin of superconductivity. As the spin excitations in superconducting $FeTe_{0.51}Se_{0.49}$ emanate from a position closer to the $(0.5\ 0.5\ 0)_T$ than do those from non-superconducting $Fe_{1.04}Te_{0.73}Se_{0.27}$, it is tempting to conclude that spin excitations near $(0.5\ 0.5\ 0)_T$ are important for pairing. Unfortunately, this interpretation is clouded by the presence of the interstitial Fe in $Fe_{1.04}Te_{0.73}Se_{0.27}$ which may be pair breaking [45].

### *4.3. The spin resonance*

The origin and importance of a spin resonance in the INS spectrum is the subject of considerable debate, e.g. [182–187]. Experimentally, a resonance in the spin excitation spectrum occurring at the onset of $T_C$ was first found in the cuprates [188–191] and subsequently in the heavy fermion materials [192, 193]. A similar phenomena was also discovered in INS studies of a polycrystalline sample of $Ba_{1-x}K_xFe_2As_2$ [143]. This work was subsequently followed by observations of a spin resonance in single crystals of $BaFe_{1.84}Co_{0.16}As_2$ [144] and $BaFe_{1.9}Ni_{0.1}As_2$ [145]. Following that numerous observations of a spin resonance in various Fe-based superconductors have been made [143–145, 194, 195, 160, 174, 175, 177, 178, 196, 197, 67, 179] (see table 4).

The resonance is manifested in the INS spectrum as the appearance of new intensity below $T_C$ localized in both

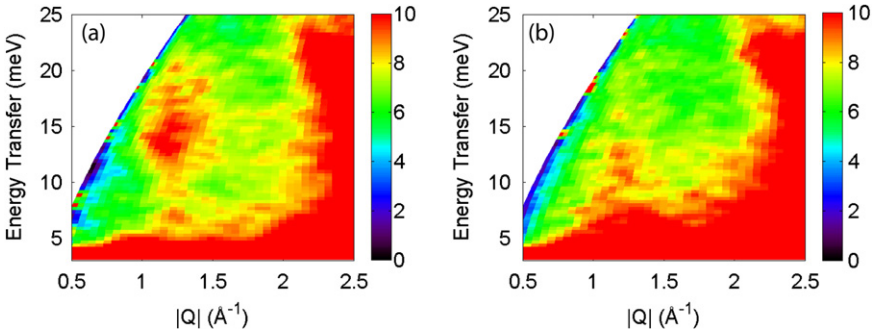


**Figure 12.** Resonant spin excitation in $Ba_{0.6}K_{0.4}Fe_2As_2$. (Reprinted by permission from Macmillan Publishers Ltd: Nature [143], copyright 2008). (a) INS data for $T < T_C$. (b) INS data for $T > T_C$. The spin resonance is visible as the bright spot in (a).

wavevector and energy. This additional intensity exhibits a temperature dependence which is strongly coupled to the onset of superconductivity (e.g. see figure 10(b)) and the spectral weight appears to arise from a gapping of the spin excitation spectrum. Theoretically, a spin resonance occurs because of the enhancement of the dynamic susceptibility through a sign change of the superconducting order parameter on different parts of the Fermi surface [182, 183, 186, 187, 198] and consequently the observation of a spin resonance is typically taken as strong evidence for an unconventional pairing symmetry such as d-wave or extended s-wave (s±).

As noted above, a spin resonance in the Fe-based family of superconductors was first observed in polycrystalline samples of $Ba_{0.6}K_{0.4}Fe_2As_2$ [143]. Figure 12 shows INS data as a function of Q and energy transfer for temperatures below (a) and above (b) $T_C$. The resonance is the clearly identifiable spot of intensity below $T_C$. The resonant intensity appears at a wavevector consistent with $(\frac{1}{2}\ \frac{1}{2}\ 0)_T$ suggesting that the resonance occurs due to dynamic spin correlations in the tetragonal basal plane. In-plane spin correlations are consistent with NMR measurements in optimally doped $Ba_{0.6}K_{0.4}Fe_2As_2$ [199]. However, a unique identification of the wavevector is not possible without INS measurements on a single crystal specimen.

The discovery of superconductivity on replacement of Fe with Co in $BaFe_2As_2$ [18] allowed significant progress to be made due to the availability of relatively large single crystals. Shortly thereafter, INS experiments were reported on optimally doped $BaFe_{1.84}Co_{0.16}As_2$ ($T_C$ = 22 K) [144] and $BaFe_{1.9}Ni_{0.1}As_2$ ($T_C$ = 20 K) [145]. These measurements confirmed the first results on $Ba_{0.6}K_{0.4}Fe_2As_2$ and provided several new pieces of information. The excitations of $BaFe_{1.84}Co_{0.16}As_2$ were explored with a combination of time-of-flight and triple-axis techniques which located the spin excitations with high confidence at the $(0.5\ 0.5\ L)_T$ wavevectors [144]. Triple-axis measurements on $BaFe_{1.9}Ni_{0.1}As_2$ performed in the $(HHL)_T$ plane are also consistent with this wavevector [145]. As discussed above, the $c$-axis spin correlations were found in both cases to be much weaker than those observed in the parent compounds. The resonance appears to mimic the behavior of the spin excitations in this regard with only a weak dependence on $L$ in $BaFe_{1.84}Co_{0.16}As_2$ [144] and perhaps a somewhat stronger $L$-dependence in $BaFe_{1.9}Ni_{0.1}As_2$ [145, 194]. The work in both materials showed the appearance of a gap in the spin fluctuation spectrum coincident with the onset of $T_C$ and, thus, the spectral weight in the resonance appeared to be derived from a redistribution of spectral weight from low energy to the resonance position.

The opening of the superconducting gap with temperature and the relationship to superconductivity was more completely explored in $BaFe_{1.9}Ni_{0.1}As_2$ [194]. The authors argue that the opening of a gap in the spin excitations spectrum is temperature dependent and evolves in the same manner as angle resolved photoemission [200]. The idea that the opening of a gap in the spin excitation spectrum mirrors the opening of the superconducting gap was further clarified by INS measurements of an optimally doped sample with composition $BaFe_{1.85}Co_{0.15}As_2$ ($T_C$ = 25 K) where the temperature dependence of the resonance energy was found to be the same as that of the superconducting gap [160].

A spin resonance has also been observed in several other Fe-based superconductors including: $LaFeAsO_{0.918}F_{0.082}$ [197] and several samples in the $FeTe_{1-x}Se_x$ series [174, 175, 177, 178, 196, 179]. Measurements on polycrystalline samples of $LaFeAsO_{0.918}F_{0.082}$ show the existence of the resonance in the 1111 materials with a resonance energy of 12.9(1) meV corresponding to 5.2 $k_BT_C$ [197]. In the $FeTe_{1-x}Se_x$ series, the observation of a spin resonance was first reported by Mook *et al* [174] and Qiu *et al* [175], (see figure 13). Both studies showed a resonance located at the $(0.5\ 0.5\ 0)_T$ position in the (HHL) scattering plane; a position in common with that in the 122 materials but not at the position of the ordering wavevector in the parent compound FeTe [131, 44, 117]. Qiu *et al*, were able to show that the resonance was 2D in character and hence was due to in-plane spin correlations [175]. As discussed above, the normal state spin fluctuations out of which the resonance evolves are peaked near $(\frac{1}{2}\ \frac{1}{2}\ 0)_T$ but are actually incommensurate in the orthogonal direction [176]. Further studies have subsequently examined the relationship of the location of the spin resonance and normal state incommensurate spin excitations [178, 177, 179].

As the origin and importance of the resonance are the subjects of considerable debate, probing the nature of the spin resonance as a function of a various tuning parameters is

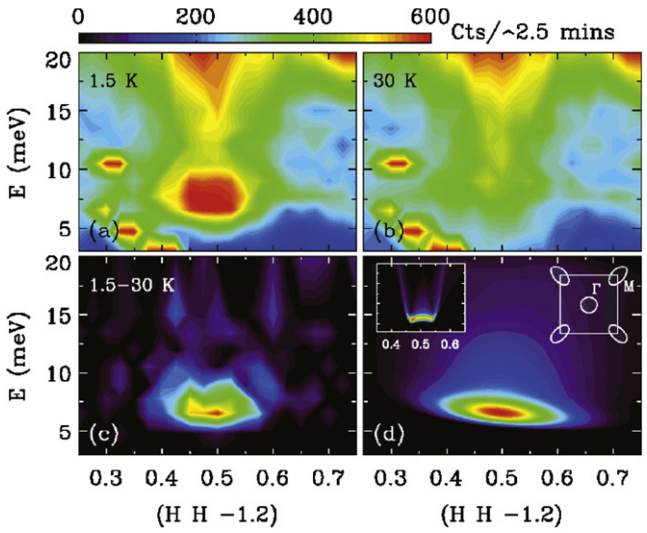


**Figure 13.** Spin resonance in $FeTe_{0.6}Se_{0.4}$ (reprinted with permission from [175], copyright 2009 the American Physical Society). (a) and (b) shows the spin excitation spectrum as a function of **Q** and energy at 1.5 and 30 K respectively. (c) shows the resonant intensity as determined by the difference between the 1.5 and 30 K spectra. (d) A theoretical calculation for the resonant intensity as described in [175].

critical. To date this has been done with both chemical doping and applied magnetic fields in the Fe-based superconductors. Underdoped samples of $BaFe_{1.92}Co_{0.08}As_2$ ($T_C = 11$ K, $T_N = 58$ K) [67] (see figure 10) and $BaFe_{1.906}Co_{0.094}As_2$ ($T_C = 17$, $T_N = 47$ K) [66] both show the presence of a spin resonance coexisting with the spin waves of the magnetically ordered state. Analysis of the spin waves in $BaFe_{1.92}Co_{0.08}As_2$ are consistent with a gapped spectrum (for temperatures below $T_N$ and above $T_C$) as in the parent compounds [143]. Note that the observation of a gap is complicated by the presence of significant damping. Below $T_C$, there does not appear to be a suppression of spectral weight at energies below the resonance unless such suppression occurs below ~2 meV. Thus, unlike the optimally doped materials, the spectral weight for the resonance appears to derive from a source other than the gapping of the spin fluctuations below $T_C$. Interestingly, the static antiferromagnetic order may prove to be the origin of the spectral weight in the resonance as the magnetic Bragg peaks exhibit suppressed spectral weight below $T_C$ [67, 66] (see figure 3). A similar interplay between magnetism and superconductivity has been seen in heavy fermion superconductor $UPd_2Al_3$ [70].

One prominent viewpoint is that the spin resonance is a singlet–triplet excitation. This hypothesis can be tested by experiments conducted with applied magnetic field which should in principle lift the degeneracy of the triplet excited state [191, 204]. The effect of an applied magnetic field has been studied in $BaFe_{1.9}Ni_{0.1}As_2$ [205] and $FeTe_{0.5}Se_{0.5}$ [196, 175]. No change in the resonance was seen in $FeTe_{0.6}Se_{0.4}$ in the presence of a 7 T applied magnetic field [175] while measurements on $FeTe_{0.5}Se_{0.5}$ showed an intensity change in a 7 T field with no detectable change in resonance energy [196]. The change in the resonance intensity is attributed to changes in the superconducting volume [196]. The resonance in $BaFe_{1.9}Ni_{0.1}As_2$ has been measured in magnetic fields up to 14.5 T [205]. Comparing the 14.5 T data to the zero field data, the resonance is reduced in intensity, shifted downward in energy, and slightly broadened. The experimental data is consistent with the resonance being directly correlated with the superconducting gap [205]. Very recently (just prior to final submission of this article), measurements of the $FeSe_{0.4}Te_{0.6}$ in applied fields up to 14 T have been reported [206]. These measurements appear to show a field induced peak splitting and may be consistent with a singlet–triplet excitation. Certainly, further experimental work in this area is needed to definitively establish whether or not the spin resonance is a singlet–triplet excitation (in some or all of the Fe-based superconductors).

The meaning of the resonance can be examined further by various scaling approaches. One method of scaling is to simply scale the spin resonance energy by $T_C$. The scaling of the spin resonance to $k_B T_C$ and, where available, to twice the maximum superconducting gap is shown in table 4. The scaling with $T_C$ in the cuprates is typically quoted to be around $5k_B T_C$ [207]. The scaling with $T_C$ observed in the Fe-based superconductors, ~4.9 $k_B T_C$ (see table 4), is consistent with that in the cuprates. In contrast in the heavy fermion materials such scaling is not applicable as exemplified by $CeCoIn_5$ (values included in table 4 for reference) [193]. Stock, *et al* [193] point this out and suggested an alternative scaling whereby the resonance energy is scaled by twice the maximum superconducting gap ($E_r/2\Delta$). (Note: a related scaling was also suggested by Mourachkine [208].) This scaling gives agreement for three different d-wave superconductors, $Bi_2Sr_2CaCu_2O_{8+\delta}$, $CeCoIn_5$, and $UPd_2Al_3$ [193]. This scaling also was found to work in $Ba_{0.6}K_{0.4}Fe_2As_2$ [143]. Subsequently, the scaling of the resonance energy with the gap has been examined systematically in a large number of unconventional superconductors, including several Fe-based superconductors, yielding a universal value of ~0.64 [209]. As shown in table 4, in cases where the gap is available, this scaling is also observed in the Fe-based materials. This provides a graphic demonstration of the link between the superconducting gap and spin fluctuations in unconventional superconducting materials.

A commonly held view of the superconducting resonance is that the enhancement of intensity in the INS spectra is due to a sign change of the superconducting order parameter on different parts of the Fermi surface. Thus, in the cuprates and heavy fermion materials the observation of a spin resonance is typically taken as evidence for d-wave superconductivity. Early theoretical investigations of Fe-based superconductors suggested an $s_\pm$ wave pairing symmetry [90, 210]. The observation of a spin resonance in $Ba_{0.6}K_{0.4}Fe_2As_2$ [143] where photoemission measurements found no nodes in the superconducting gap [201] are naturally explained within an $s_\pm$ picture. Moreover, the energy of the resonance seems to agree reasonably with theoretical calculations for the neutron spectra [211–213] in a number of materials [143, 144, 160]. An alternative point of view has been presented by Onari *et al* [214]. They argue that a sign change in the superconducting

order parameter is not needed to give rise to a peak in the dynamic susceptibility and that the spin resonance feature can be understood assuming $s_{++}$ pairing symmetry. Future experimental and theoretical investigation of this proposal would be interesting.

## 5. Summary

The first evidence of the interplay between magnetism and superconductivity in the Fe-based superconductors was the presence of magnetism in the concentration dependent phase diagrams. The parent compounds exhibit a magnetically ordered state which is suppressed with doping and superconductivity appears at higher concentrations. While this general behavior is common for different materials, the behavior near the boundary between superconductivity and magnetism is material specific. The magnetically ordered state of some materials vanish abruptly with the appearance of superconductivity, in others superconductivity emerges precisely as the magnetic order is destroyed, and still others exhibit coexistence between the magnetically ordered and superconducting states. This issue of microscopic phase coexistence has been most carefully examined in doped $BaFe_2As_2$ with most measurements supporting phase coexistence in $Ba(Fe_{1-x}Co_x)_2As_2$ while phase separation seems to occur in $Ba_{1-x}K_xFe_2As_2$.

The magnetic structure of the parent compounds indicate an identical in-plane spin arrangement in the 1111, 122, and 111 materials although the stacking of neighboring planes along the $c$-axis is material dependent. This stripe-like structure consists of moments oriented along the orthorhombic $a$-axis stacked antiferromagnetically along $a$ and ferromagnetically along $b$. Several explanations of this magnetic structure have been proposed including Fermi surface nesting, local moments interacting via frustrated superexchange interactions, local moments interacting via longer range interactions primarily of an itinerant nature, and orbital ordering. The ordered Fe moments are very small in the RFeAsO parent compounds and, interestingly, $^{57}$Fe Mössbauer measurements indicate a very similar magnetic moment for all measured rare earths while neutron diffraction indicates very different behavior particularly for the case of R = Ce where a much larger moment is observed (a similar effect is also seen in $\mu$SR). Curiously, the exact opposite behavior is seen in the $AFe_2As_2$ parent compounds where neutron diffraction shows a very similar Fe moment for all values of A while $^{57}$Fe Mössbauer shows strong variation with A with very different internal fields observed for A = Ba and A = Sr, Eu. The magnetic structure of the 11 materials is a particularly interesting case as the magnetic structure is found to be quite different than the 1111 and 122 materials despite a very similar Fermi surface topology seemingly inconsistent with a picture of magnetic order occurring purely as a result of a nesting instability.

While many of the details still remain unknown the investigations of the spin excitations described above have already established much of the basic behavior. Namely, that the interactions in the magnetically ordered parent compounds have been determined to be anisotropic 3D interactions. With doping the correlations along the $c$-axis appear to be more quickly suppressed so that in optimally doped samples where no long range magnetic order is present the spin excitations appear to be 2D in character much as in the normal state of the parent compounds. This latter behavior is not entirely unexpected from the magnetic phase diagrams of the Fe-based materials since the paramagnetic state of the parent compounds appears to be the same paramagnetic state out of which superconductivity develops in the optimally doped superconducting materials. In the superconducting materials, spin fluctuations near $(0.5\ 0.5\ 0)_T$ have been found in all cases investigated. These investigations further show the development of a spin resonance below $T_C$ demonstrating a direct interplay between magnetism and superconductivity. For now the observation of the spin resonance in the Fe-based materials appears to support a $s_\pm$ pairing symmetry, but this issue is far from settled. In the few cases studied by INS the spin fluctuations seem to weaken considerably and disappear in the overdoped regime. Certainly much work remains to be done in these fascinating materials.

## Acknowledgments

The authors would like to extend our sincere thanks to all of our collaborators. In particular we thank E Goremychkin, M McGuire, T Maier, D Mandrus, S Nagler, R Osborn, B Sales, A Sefat, and D Singh. We would also like to thank our colleagues who have graciously allowed us to reproduce their work here. Work at ORNL was supported by the Scientific User Facilities Division Office of Basic Energy Sciences, DOE.

## References

[1] Kamihara Y, Watanabe T, Hirano M and Hosono H 2008 Iron-based layered superconductor $La[O_{1-x}F_x]FeAs$ ($x = 0.05$–$0.12$) with $T_C = 26$ K *J. Am. Chem. Soc.* **130** 3296

[2] Ren Z A *et al* 2008 Superconductivity in the iron-based F-doped layered quaternary compound $Nd[O_{1-x}F_x]FeAs$ *Europhys. Lett.* **82** 57002

[3] Ren Z A, Yang J, Lu W, Yi W, Che G C, Dong X L, Sun L L and Zhao Z X 2008 Superconductivity at 52 K in iron based F doped layered quaternary compound $Pr[O_{1-x}F_x]FeAs$ *Mater. Res. Innov.* **12** 105–6

[4] Ren Z A *et al* 2008 Superconductivity at 55 K in iron-based F-doped layered quaternary compound $Sm[O_{1-x}F_x]FeAs$ *Chin. Phys. Lett.* **25** 2215–6

[5] Chen G F, Li Z, Wu D, Li G, Hu W Z, Dong J, Zheng P, Luo J L and Wang N L 2008 Superconductivity at 41 K and its competition with spin-density-wave instability in layered $CeO_{1-x}F_xFeAs$ *Phys. Rev. Lett.* **100** 247002

[6] Cheng P, Fang L, Yang H, Zhu X, Mu G, Luo H, Wang Z and Wen H 2008 Superconductivity at 36 K in gadolinium–arsenide oxides $GdO_{1-x}F_xFeAs$ *Sci. Chin.* G **51** 719–22

[7] Kadowaki K, Goya A, Mochiji T and Chong S V 2009 Superconductivity and magnetism in $REFeAsO_{1-x}F_x$ (RE = rare earth elements) *J. Phys.: Conf. Ser.* **150** 4

[8] Khlybov E, Omelyanovsky O, Zaleski A, Sadakov A, Gizatulin D, Kulikova L, Kostuleva I and Pudalov V 2009 Magnetic and superconducting properties of FeAs-based high-Tc superconductors with Gd *JETP Lett.* **90** 387–90

[9] Bos J W G, Penny G B S, Rodgers J A, Sokolov D A, Huxley A D and Attfield J P 2008 High pressure synthesis of late rare earth RFeAs(O, F) superconductors; R = Tb and Dy *Chem. Commun.* 3634–5

[10] Wang C *et al* 2008 Thorium-doping-induced superconductivity up to 56 K in $Gd_{1-x}Th_xFeAsO$ *Europhys. Lett.* **83** 67006

[11] Ren Z A *et al* 2008 Superconductivity and phase diagram in iron-based arsenic-oxides $ReFeAsO_{1-\delta}$ (Re = rare-earth metal) without fluorine doping *Europhys. Lett.* **83** 17002

[12] Miyazawa K, Kihou K, Shirage P M, Lee C H, Kito H, Eisaki H and Iyo A 2009 Superconductivity above 50 K in $LnFeAsO_{(1-y)}$ (Ln = Nd, Sm, Gd, Tb, and Dy) synthesized by high-pressure technique *J. Phys. Soc. Japan* **78** 034712

[13] Kito H, Eisaki H and Iyo A 2008 Superconductivity at 54 K in F-free $NdFeAsO_{1-y}$ *J. Phys. Soc. Japan* **77** 063707

[14] Yang J *et al* 2008 Superconductivity at 53.5 K in $GdFeAsO_{1-\delta}$ *Supercond. Sci. Technol.* **21** 082001

[15] de la Cruz C *et al* 2008 Magnetic order close to superconductivity in the iron-based layered $LaO_{1-x}F_xFeAs$ systems *Nature* **453** 899–902

[16] Rotter M, Tegel M and Johrendt D 2008 Superconductivity at 38 K in the iron arsenide $(Ba_{1-x}K_x)Fe_2As_2$ *Phys. Rev. Lett.* **101** 107006

[17] Sefat A S, Huq A, McGuire M A, Jin R Y, Sales B C, Mandrus D, Cranswick L M D, Stephens P W and Stone K H 2008 Superconductivity in $LaFe_{1-x}Co_xAsO$ *Phys. Rev.* B **78** 104505

[18] Sefat A S, Jin R Y, McGuire M A, Sales B C, Singh D J and Mandrus D 2008 Superconductivity at 22 K in Co-doped $BaFe_2As_2$ crystals *Phys. Rev. Lett.* **101** 117004

[19] Li L J *et al* 2009 Superconductivity induced by Ni doping in $BaFe_2As_2$ single crystals *New J. Phys.* **11** 025008

[20] Ni N, Thaler A, Kracher A, Yan J Q, Bud'ko S L and Canfield P C 2009 Phase diagrams of $Ba(Fe_{1-x}M_x)_2As_2$ single crystals (M = Rh and Pd) *Phys. Rev.* B **80** 024511

[21] Han F *et al* 2009 Superconductivity and phase diagrams of the 4d- and 5d-metal-doped iron arsenides $SrFe_{2-x}M_xAs_2$ (M = Rh, Ir, Pd) *Phys. Rev.* B **80** 024506

[22] Paulraj S, Sharma S, Bharathi A, Satya A T, Chandra S, Hariharan Y and Sundar C S 2009 Superconductivity in Ru substituted $BaFe_{2-x}Ru_xAs_2$ arXiv:0902.2728

[23] Qi Y P, Wang L, Gao Z S, Wang D L, Zhang X P and Ma Y W 2009 Superconductivity induced by doping Ru in $SrFe_{2-x}Ru_xAs_2$ *Physica* C **469** 1921–4

[24] Canfield P C, Bud'ko S L, Ni N, Yan J Q and Kracher A 2009 Decoupling of the superconducting and magnetic/structural phase transitions in electron-doped $BaFe_2As_2$ *Phys. Rev.* B **80** 060501

[25] Sefat A S, Singh D J, VanBebber L H, Mozharivskyj Y, McGuire M A, Jin R Y, Sales B C, Keppens V and Mandrus D 2009 Absence of superconductivity in hole-doped $BaFe_{2-x}Cr_xAs_2$ single crystals *Phys. Rev.* B **79** 224524

[26] Li Y K, Lin X, Zhou T, Shen J Q, Tao Q, Cao G H and Xu Z A 2009 Superconductivity induced by Ni doping in SmFe1-xNixAsO *J. Phys.: Condens. Matter* **21** 355702

[27] Qi Y P, Gao Z S, Wang L, Wang D L, Zhang X P and Ma Y W 2008 Superconductivity in co-doped SmFeAsO *Supercond. Sci. Technol.* **21** 115016

[28] Qi Y P, Wang L, Gao Z S, Wang D L, Zhang X P, Zhang Z Y and Ma Y W 2009 Superconductivity in Ir-doped $LaFe_{1-x}Ir_xAsO$ *Phys. Rev.* B **80** 054502

[29] Bukowski Z, Weyeneth S, Puzniak R, Moll P, Katrych S, Zhigadlo N D, Karpinski J, Keller H and Batlogg B 2009 Superconductivity at 23 K and low anisotropy in Rb-substituted $BaFe_2As_2$ single crystals *Phys. Rev.* B **79** 104521

[30] Sasmal K, Lv B, Lorenz B, Guloy A M, Chen F, Xue Y Y and Chu C W 2008 Superconducting Fe-based compounds $(A_{1-x}Sr_x)Fe_2As_2$ with A = K and Cs with transition temperatures up to 37 K *Phys. Rev. Lett.* **101** 107007

[31] Wu G, Chen H, Wu T, Xie Y L, Yan Y J, Liu R H, Wang X F, Ying J J and Chen X H 2008 Different resistivity response to spin-density wave and superconductivity at 20 K in $Ca_{1-x}Na_xFe_2As_2$ *J. Phys.: Condens. Matter* **20** 422201

[32] Jeevan H S, Hossain Z, Kasinathan D, Rosner H, Geibel C and Gegenwart P 2008 High-temperature superconductivity in $Eu_{0.5}K_{0.5}Fe_2As_2$ *Phys. Rev.* B **78** 092406

[33] Qi Y P, Gao Z S, Wang L, Wang D L, Zhang X P and Ma Y W 2008 Superconductivity at 34.7 K in the iron arsenide $Eu_{0.7}Na_{0.3}Fe_2As_2$ *New J. Phys.* **10** 123003

[34] Chu J H, Analytis J G, Kucharczyk C and Fisher I R 2009 Determination of the phase diagram of the electron-doped superconductor $Ba(Fe_{1-x}Co_x)_2As_2$ *Phys. Rev.* B **79** 014506

[35] Saha S R, Butch N P, Kirshenbaum K and Paglione J 2009 Evolution of bulk superconductivity in $SrFe_2As_2$ with Ni substitution *Phys. Rev.* B **79** 224519

[36] Kumar N, Nagalakshmi R, Kulkarni R, Paulose P L, Nigam A K, Dhar S K and Thamizhavel A 2009 Anisotropic magnetic and superconducting properties of $CaFe_{2-x}Co_xAs_2$ ($x = 0, 0.06$) single crystals *Phys. Rev.* B **79** 012504

[37] Tapp J H, Tang Z J, Lv B, Sasmal K, Lorenz B, Chu P C W and Guloy A M 2008 LiFeAs: an intrinsic FeAs-based superconductor with $T_C = 18$ K *Phys. Rev.* B **78** 060505

[38] Wang X C, Liu Q Q, Lv Y X, Gao W B, Yang L X, Yu R C, Li F Y and Jin C Q 2008 The superconductivity at 18 K in LiFeAs system *Solid State Commun.* **148** 538–40

[39] Pitcher M J, Parker D R, Adamson P, Herkelrath S J C, Boothroyd A T, Ibberson R M, Brunelli M and Clarke S J 2008 Structure and superconductivity of LiFeAs *Chem. Commun.* 5918–20

[40] Chu C W, Chen F, Gooch M, Guloy A M, Lorenz B, Lv B, Sasmal K, Tang Z J, Tapp J H and Xue Y Y 2009 The synthesis and characterization of LiFeAs and NaFeAs *Physica* C **469** 326–31

[41] Yeh K W *et al* 2008 Tellurium substitution effect on superconductivity of the $\alpha$-phase iron selenide *Europhys. Lett.* **84** 37002

[42] Hsu F C *et al* 2008 Superconductivity in the PbO-type structure $\alpha$-FeSe *Proc. Natl Acad. Sci. USA* **105** 14262–4

[43] Subedi A, Zhang L J, Singh D J and Du M H 2008 Density functional study of FeS, FeSe, and FeTe: electronic structure, magnetism, phonons, and superconductivity *Phys. Rev.* B **78** 134514

[44] Bao W *et al* 2009 Tunable $(\delta\pi, \delta\pi)$-type antiferromagnetic order in $\alpha$-Fe(Te, Se) superconductors *Phys. Rev. Lett.* **102** 247001

[45] Zhang L J, Singh D J and Du M H 2009 Density functional study of excess Fe in $Fe_{1+x}Te$: magnetism and doping *Phys. Rev.* B **79** 012506

[46] Zhu X Y, Han F, Mu G, Cheng P, Shen B, Zeng B and Wen H H 2009 Transition of stoichiometric $Sr_2VO_3FeAs$ to a superconducting state at 37.2 K *Phys. Rev.* B **79** 220512

[47] Chen G F, Xia T-L, Yang H X, Li J Q, Zheng P, Luo J L and Wang N L 2009 Possible high temperature superconductivity in a Ti-doped AScFeAsO (A = Ca, Sr) system *Supercond. Sci. Technol.* **22** 072001

[48] Boeri L, Dolgov O V and Golubov A A 2008 Is $LaFeAsO_{1-x}F_x$ an electron–phonon superconductor? *Phys. Rev. Lett.* **101** 026403

[49] Christianson A D *et al* 2008 Phonon density of states of $LaFeAsO_{1-x}F_x$ *Phys. Rev. Lett.* **101** 157004

[50] McGuire M A *et al* 2008 Phase transitions in LaFeAsO: structural, magnetic, elastic, and transport properties, heat capacity and Mössbauer spectra *Phys. Rev.* B **78** 094517

[51] Nomura T, Kim S W, Kamihara Y, Hirano M, Sushko P V, Kato K, Takata M, Shluger A L and Hosono H 2008 Crystallographic phase transition and high-$T_c$ superconductivity in LaFeAsO:F *Supercond. Sci. Technol.* **21** 125028

[52] Luetkens H *et al* 2009 The electronic phase diagram of the $LaO_{1-x}F_xFeAs$ superconductor *Nat. Mater.* **8** 305–9

[53] Zhao J *et al* 2008 Structural and magnetic phase diagram of $CeFeAsO_{1-x}F_x$ and its relation to high-temperature superconductivity *Nat. Mater.* **7** 953–9

[54] Drew A J *et al* 2009 Coexistence of static magnetism and superconductivity in $SmFeAsO_{1-x}F_x$ as revealed by muon spin rotation *Nat. Mater.* **8** 310–4

[55] Khasanov R *et al* 2009 Coexistence of incommensurate magnetism and superconductivity in $Fe_{1+y}Se_xTe_{1-x}$ *Phys. Rev.* B **80** 140511

[56] Rotundu C R, Keane D T, Freelon B, Wilson S D, Kim A, Valdivia P N, Bourret-Courchesne E and Birgeneau R J 2009 Phase diagram of the $PrFeAsO_{1-x}F_x$ superconductor arXiv:0907.1308

[57] Margadonna S, Takabayashi Y, Mcdonald M T, Brunelli M, Wu G, Liu R H, Chen X H and Prassides K 2009 Crystal structure and phase transitions across the metal–superconductor boundary in the $SmFeAsO_{1-x}F_x$ ($0 <= x <= 0.20$) family *Phys. Rev.* B **79** 014503

[58] Chen G F, Li Z, Wu D, Dong J, Li G, Hu W Z, Zheng P, Luo J L and Wang N L 2008 Element substitution effect in transition metal oxypnictide $Re(O_{1-x}F_x)TAs$ (Re = rare earth, T = transition metal) *Chin. Phys. Lett.* **25** 2235–8

[59] Rotter M, Tegel M, Johrendt D, Schellenberg I, Hermes W and Pottgen R 2008 Spin-density-wave anomaly at 140 K in the ternary iron arsenide $BaFe_2As_2$ *Phys. Rev.* B **78** 020503

[60] Huang Q, Qiu Y, Bao W, Green M A, Lynn J W, Gasparovic Y C, Wu T, Wu G and Chen X H 2008 Neutron-diffraction measurements of magnetic order and a structural transition in the parent $BaFe_2As_2$ compound of FeAs-based high-temperature superconductors *Phys. Rev. Lett.* **101** 257003

[61] Kofu M, Qiu Y, Bao W, Lee S H, Chang S, Wu T, Wu G and Chen X H 2009 Neutron scattering investigation of the magnetic order in single crystalline $BaFe_2As_2$ *New J. Phys.* **11** 055001

[62] Rotter M, Pangerl M, Tegel M and Johrendt D 2008 Superconductivity and crystal structures of $(Ba_{1-x}K_x)Fe_2As_2$ ($x = 0$–1) *Angew. Chem. Int. Edn* **47** 7949–52

[63] Chen H *et al* 2009 Coexistence of the spin-density wave and superconductivity in $Ba_{1-x}K_xFe_2As_2$ *Europhys. Lett.* **85** 17006

[64] Wang X F, Wu T, Wu G, Liu R H, Chen H, Xie Y L and Chen X H 2009 The peculiar physical properties and phase diagram of $BaFe_{2-x}Co_xAs_2$ single crystals *New J. Phys.* **11** 045003

[65] Ni N, Tillman M E, Yan J Q, Kracher A, Hannahs S T, Bud'ko S L and Canfield P C 2008 Effects of Co substitution on thermodynamic and transport properties and anisotropic $H_{c2}$ in $Ba(Fe_{1-x}Co_x)_2As_2$ single crystals *Phys. Rev.* B **78** 214515

[66] Pratt D K, Tian W, Kreyssig A, Zarestky J L, Nandi S, Ni N, Bud'ko S L, Canfield P C, Goldman A I and Mcqueeney R J 2009 Coexistence of competing antiferromagnetic and superconducting phases in the underdoped $Ba(Fe_{0.953}Co_{0.047})_2As_2$ compound using x-ray and neutron scattering techniques *Phys. Rev. Lett.* **103** 087001

[67] Christianson A D, Lumsden M D, Nagler S E, MacDougall G J, McGuire M A, Sefat A S, Jin R, Sales B C and Mandrus D 2009 Static and dynamic magnetism in underdoped superconductor $BaFe_{1.92}Co_{0.08}As_2$ *Phys. Rev. Lett.* **103** 087002

[68] Chevrel R, Hirrien M and Sergent M 1986 Superconducting Chevrel phases: prospects and perspectives *Polyhedron* **5** 87–94

[69] Müller K-H and Narozhnyi V N 2001 Interaction of superconductivity and magnetism in borocarbide superconductors *Rep. Prog. Phys.* **64** 943

[70] Metoki N, Haga Y, Koike Y and Onuki Y 1998 Superconducting energy gap observed in the magnetic excitation spectra of a heavy fermion superconductor $UPd_2Al_3$ *Phys. Rev. Lett.* **80** 5417

[71] Isaacs E D, Zschack P, Broholm C L, Burns C, Aeppli G, Ramirez A P, Palstra T T M, Erwin R W, Stücheli N and Bucher E 1995 Antiferromagnetism and its relation to the superconducting phases of $UPt_3$ *Phys. Rev. Lett.* **75** 1178

[72] Fukazawa H *et al* 2009 As-75 NMR study of hole-doped superconductor $Ba_{1-x}K_xFe_2As_2$ ($T_C$ similar or equal to 38 K) *J. Phys. Soc. Japan* **78** 033704

[73] Park J T *et al* 2009 Electronic phase separation in the slightly underdoped iron pnictide superconductor $Ba_{1-x}K_xFe_2As_2$ *Phys. Rev. Lett.* **102** 117006

[74] Inosov D S *et al* 2009 Suppression of the structural phase transition and lattice softening in slightly underdoped $Ba_{1-x}K_xFe_2As_2$ with electronic phase separation *Phys. Rev.* B **79** 224503

[75] Rotter M, Tegel M, Schellenberg I, Schappacher F M, Pottgen R, Deisenhofer J, Gunther A, Schrettle F, Loidl A and Johrendt D 2009 Competition of magnetism and superconductivity in underdoped $(Ba_{1-x}K_x)Fe_2As_2$ *New J. Phys.* **11** 025014

[76] Laplace Y, Bobroff J, Rullier-Albenque F, Colson D and Forget A 2009 Atomic coexistence of superconductivity and incommensurate magnetic order in the pnictide $Ba(Fe_{1-x}Co_x)_2As_2$ *Phys. Rev.* B **80** 140501

[77] Bernhard C *et al* 2009 Muon spin rotation study of magnetism and superconductivity in $BaFe_{2-x}Co_xAs_2$ and $Pr_{1-x}Sr_xFeAsO$ *New J. Phys.* **11** 055050

[78] Julien M H, Mayaffre H, Horvatic M, Berthier C, Zhang X D, Wu W, Chen G F, Wang N L and Luo J L 2009 Homogeneous versus inhomogeneous coexistence of magnetic order and superconductivity probed by NMR in Co- and K-doped iron pnictides *Europhys. Lett.* **87** 37001

[79] Nandi S *et al* 2010 Anomalous suppression of the orthorhombic distortion in superconducting $Ba(Fe_{1-x}Co_x)_2As_2$ *Phys. Rev. Lett.* **104** 057006

[80] Sales B C, Sefat A S, McGuire M A, Jin R Y, Mandrus D and Mozharivskyj Y 2009 Bulk superconductivity at 14 K in single crystals of $Fe_{1+y}Te_xSe_{1-x}$ *Phys. Rev.* B **79** 094521

[81] Paulose P L, Yadav C S and Subhedar K M 2009 Magnetic phase diagram of $Fe_{1+y}Te_{1-x}Se_x$ system: coexistence of spin glass behavior with superconductivity? arXiv:0907.3513

[82] Klingeler R *et al* 2010 Local antiferromagnetic correlations in the iron pnictide superconductors $LaFeAsO_{1-x}F_x$ and $Ca(Fe_{1-x}Co_x)_2As_2$ as seen via normal-state susceptibility *Phys. Rev.* B **81** 024506

[83] Wang X F, Wu T, Wu G, Chen H, Xie Y L, Ying J J, Yan Y J, Liu R H and Chen X H 2009 Anisotropy in the electrical resistivity and susceptibility of superconducting $BaFe_2As_2$ single crystals *Phys. Rev. Lett.* **102** 117005

[84] Yan J Q *et al* 2008 Structural transition and anisotropic properties of single-crystalline $SrFe_2As_2$ *Phys. Rev.* B **78** 024516

[85] Zhang G M, Su Y H, Lu Z Y, Weng Z Y, Lee D H and Xiang T 2009 Universal linear-temperature dependence of static magnetic susceptibility in iron pnictides *Europhys. Lett.* **86** 37006

[86] Sales B C, McGuire M A, Sefat A S and Mandrus D 2010 A model of the normal state susceptibility and transport properties of $Ba(Fe_{1-x}Co_x)_2As_2$: an explanation of the increase of magnetic susceptibility with temperature *Physica* C **470** 304

[87] McGuire T R and Kriessman C J 1952 The magnetic susceptibility of chromium *Phys. Rev.* **85** 452

[88] Huang Q, Zhao J, Lynn J W, Chen G F, Luo J L, Wang N L and Dai P C 2008 Doping evolution of antiferromagnetic order and structural distortion in $LaFeAsO_{1-x}F_x$ *Phys. Rev.* B **78** 054529

[89] Singh D J and Du M H 2008 Density functional study of $LaFeAsO_{1-x}F_x$: a low carrier density superconductor near itinerant magnetism *Phys. Rev. Lett.* **100** 237003

[90] Mazin I I, Singh D J, Johannes M D and Du M H 2008 Unconventional superconductivity with a sign reversal in the order parameter of $LaFeAsO_{1-x}F_x$ *Phys. Rev. Lett.* **101** 057003

[91] Dong J *et al* 2008 Competing orders and spin-density-wave instability in $LaO_{1-x}F_x$ FeAs *Europhys. Lett.* **83** 27006

[92] Yildirim T 2008 Origin of the 150 K anomaly in LaFeAsO: competing antiferromagnetic interactions, frustration, and a structural phase transition *Phys. Rev. Lett.* **101** 057010

[93] Ma F J, Lu Z Y and Xiang T 2009 Arsenic-bridged antiferromagnetic superexchange interactions in LaFeAsO (vol 78, art no 224517, 2008) *Phys. Rev.* B **79** 224517

[94] Si Q M and Abrahams E 2008 Strong correlations and magnetic frustration in the high $T_C$ iron pnictides *Phys. Rev. Lett.* **101** 076401

[95] Fang C, Yao H, Tsai W F, Hu J P and Kivelson S A 2008 Theory of electron nematic order in LaFeAsO *Phys. Rev.* B **77** 224509

[96] Johannes M D and Mazin I I 2009 Microscopic origin of magnetism and magnetic interactions in ferropnictides *Phys. Rev.* B **79** 220510

[97] Lee C-C, Yin W-G and Ku W 2009 Ferro-orbital order and strong magnetic anisotropy in the parent compounds of iron-pnictide superconductors *Phys. Rev. Lett.* **103** 267001

[98] Chen Y, Lynn J W, Li J, Li G, Chen G F, Luo J L, Wang N L, Dai P C, de la Cruz C and Mook H A 2008 Magnetic order of the iron spins in NdFeAsO *Phys. Rev.* B **78** 064515

[99] Zhao J *et al* 2008 Lattice and magnetic structures of PrFeAsO, $PrFeAsO_{0.85}F_{0.15}$, and $PrFeAsO_{0.85}$ *Phys. Rev.* B **78** 132504

[100] Ryan D H, Cadogan J M, Ritter C, Canepa F, Palenzona A and Putti M 2009 Coexistence of long-ranged magnetic order and superconductivity in the pnictide superconductor $SmFeAsO_{1-x}F_x$ ($x = 0, 0.15$) *Phys. Rev.* B **80** 220503

[101] Kimber S A J *et al* 2008 Magnetic ordering and negative thermal expansion in PrFeAsO *Phys. Rev.* B **78** 140503

[102] Qiu Y *et al* 2008 Crystal structure and antiferromagnetic order in $NdFeAsO_{1-x}F_x$ ($x = 0.0$ and 0.2) superconducting compounds from neutron diffraction measurements *Phys. Rev. Lett.* **101** 257002

[103] Klauss H H *et al* 2008 Commensurate spin density wave in LaFeAsO: a local probe study *Phys. Rev. Lett.* **101** 077005

[104] Kitao S, Kobayashi Y, Higashitaniguchi S, Saito M, Kamihara Y, Hirano M, Mitsui T, Hosono H and Seto M 2008 Spin ordering in LaFeAsO and its suppression in superconductor $LaFeAsO_{0.89}F_{0.11}$ probed by Mössbauer spectroscopy *J. Phys. Soc. Japan* **77** 103706

[105] Sanchez D R, Alzamora M, Munevar J, Wang N L, Cheng G F and Baggio-Saitovitch E 2009 Mössbauer study of superconducting $NdFeAsO_{0.88}F_{0.12}$ and its parent compound NdFeAsO *J. Phys.: Condens. Matter* **21** 455701

[106] McGuire M A, Hermann R P, Sefat A S, Sales B C, Jin R Y, Mandrus D, Grandjean F and Long G J 2009 Influence of the rare-earth element on the effects of the structural and magnetic phase transitions in CeFeAsO, PrFeAsO and NdFeAsO *New J. Phys.* **11** 025011

[107] Maeter H *et al* 2009 Interplay of rare earth and iron magnetism in RFeAsO (R = La, Ce, Pr, and Sm): muon-spin relaxation study and symmetry analysis *Phys. Rev.* B **80** 094524

[108] Aczel A A *et al* 2008 Muon-spin-relaxation studies of magnetic order and superfluid density in antiferromagnetic NdFeAsO, $BaFe_2As_2$, and superconducting $Ba_{1-x}K_xFe_2As_2$ *Phys. Rev.* B **78** 214503

[109] Carlo J P *et al* 2009 Static magnetic order and superfluid density of RFeAs(O, F) (R = La, Nd, Ce) and LaFePO studied by muon spin relaxation: unusual similarities with the behavior of cuprate superconductors *Phys. Rev. Lett.* **102** 087001

[110] Su Y *et al* 2009 Antiferromagnetic ordering and structural phase transition in $Ba_2Fe_2As_2$ with Sn incorporated from the growth flux *Phys. Rev.* B **79** 064504

[111] Zhao J, Ratcliff W, Lynn J W, Chen G F, Luo J L, Wang N L, Hu J P and Dai P C 2008 Spin and lattice structures of single-crystalline $SrFe_2As_2$ *Phys. Rev.* B **78** 140504

[112] Kaneko K, Hoser A, Caroca-Canales N, Jesche A, Krellner C, Stockert O and Geibel C 2008 Columnar magnetic structure coupled with orthorhombic distortion in the antiferromagnetic iron arsenide $SrFe_2As_2$ *Phys. Rev.* B **78** 212502

[113] Jesche A *et al* 2008 Strong coupling between magnetic and structural order parameters in $SrFe_2As_2$ *Phys. Rev.* B **78** 180504

[114] Tegel M, Rotter M, Weiss V, Schappacher F, Pottgen R and Johrendt D 2008 Structural and magnetic phase transitions in the ternary iron arsenides $SrFe_2As_2$ and $EuFe_2As_2$ *J. Phys.: Condens. Matter* **20** 452201

[115] Goldman A I, Argyriou D N, Ouladdiaf B, Chatterji T, Kreyssig A, Nandi S, Ni N, Bud'ko S L, Canfield P C and Mcqueeney R J 2008 Lattice and magnetic instabilities in $CaFe_2As_2$: a single-crystal neutron diffraction study *Phys. Rev.* B **78** 100506

[116] Raffius H, Mörsen E, Mosel B D, Müller-Warmuth W, Jeitschko W, Terbüchte L and Vomhof T 1993 Magnetic properties of ternary lanthanoid transition metal arsenides studied by Mössbauer and susceptibility measurements *J. Phys. Chem. Solids* **54** 135

[117] Li S L *et al* 2009 First-order magnetic and structural phase transitions in $Fe_{1+y}Se_xTe_{1-x}$ *Phys. Rev.* B **79** 054503

[118] Li S L, de la Cruz C, Huang Q, Chen G F, Xia T L, Luo J L, Wang N L and Dai P C 2009 Structural and magnetic phase transitions in $Na_{1-\delta}FeAs$ *Phys. Rev.* B **80** 020504

[119] Lynn J W and Dai P C 2009 Neutron studies of the iron-based family of high T-C magnetic superconductors *Physica* C **469** 469–76

[120] Ni N, Nandi S, Kreyssig A, Goldman A I, Mun E D, Bud'ko S L and Canfield P C 2008 First-order structural phase transition in $CaFe_2As_2$ *Phys. Rev.* B **78** 014523

[121] Li H F, Tian W, Zarestky J L, Kreyssig A, Ni N, Bud'ko S L, Canfield P C, Goldman A I, Mcqueeney R J and Vaknin D 2009 Magnetic and lattice coupling in single-crystal $SrFe_2As_2$: a neutron scattering study *Phys. Rev.* B **80** 054407

[122] Bonville P, Rullier-Albenque F, Colson D and Forget A 2010 Incommensurate spin density wave in Co-doped $BaFe_2As_2$ arXiv:1002.0931

[123] Wilson S D, Yamani Z, Rotundu C R, Freelon B, Bourret-Courchesne E and Birgeneau R J 2009 Neutron diffraction study of the magnetic and structural phase transitions in $BaFe_2As_2$ *Phys. Rev.* B **79** 184519

[124] Kitagawa K, Katayama N, Ohgushi K, Yoshida M and Takigawa M 2008 Commensurate itinerant antiferromagnetism in $BaFe_2As_2$: $^{75}$As-NMR studies on a self-flux grown single crystal *J. Phys. Soc. Japan* **77** 114709

[125] Kitagawa K, Katayama N, Ohgushi K and Takigawa M 2009 Antiferromagnetism of $SrFe_2As_2$ studied by single-crystal $^{75}$As NMR *J. Phys. Soc. Japan* **78** 063706

[126] Krellner C, Burkhardt U and Geibel C 2009 Interplay between 3d and 4f magnetism in CeCoPO *Physica* B **404** 3206–9

[127] Ning F L, Ahilan K, Imai T, Sefat A S, Jin R Y, McGuire M A, Sales B C and Mandrus D 2009 Spin susceptibility, phase diagram, and quantum criticality in the eelctron-doped high $T_C$ superconductor $Ba(Fe_{1-x}Co_x)_2As_2$ *J. Phys. Soc. Japan* **78** 013711

[128] Schuster W, Mikler H and Komarek K L 1979 Transition metal-chalcogen systems, VII: the iron-selenium phase diagram *Monatsh. Chem.* **110** 1153

[129] Mcqueen T M *et al* 2009 Extreme sensitivity of superconductivity to stoichiometry in $Fe_{1+\delta}Se$ *Phys. Rev.* B **79** 014522

[130] Fang M H, Pham H M, Qian B, Liu T J, Vehstedt E K, Liu Y, Spinu L and Mao Z Q 2008 Superconductivity close to magnetic instability in $Fe(Se_{1-x}Te_x)_{0.82}$ *Phys. Rev.* B **78** 224503

[131] Fruchart D, Convert P, Wolfers P, Madar R, Senateur J P and Fruchart R 1975 Structure antiferromagnetique de $Fe_{1.125}Te$ accompagnee d'une deformation monoclinique *Mater. Res. Bull.* **10** 169

[132] Wen J, Xu G, Xu Z, Lin Z W, Li Q, Ratcliff W, Gu G and Tranquada J M 2009 Short-range incommensurate magnetic order near the superconducting phase boundary in $Fe_{1+\delta}Te_{1-x}Se_x$ *Phys. Rev.* B **80** 104506

[133] Zhang C *et al* 2009 Pressure-induced lattice collapse in the tetragonal phase of single-crystalline $Fe_{1.05}Te$ *Phys. Rev.* B **80** 144519

[134] Xia Y, Qian D, Wray L, Hsieh D, Chen G F, Luo J L, Wang N L and Hasan M Z 2009 Fermi surface topology and low-lying quasiparticle dynamics of parent $Fe_{1+x}Te/Se$ superconductor *Phys. Rev. Lett.* **103** 037002

[135] Ma F J, Ji W, Hu J P, Lu Z Y and Xiang T 2009 First-principles calculations of the electronic structure of tetragonal $\alpha$-FeTe and $\alpha$-FeSe crystals: evidence for a bicollinear antiferromagnetic order *Phys. Rev. Lett.* **102** 177003

[136] Fang C, Bernevig B A and Hu J P 2009 Theory of magnetic order in $Fe_{1+y}Te_{1-x}Se_x$ *Europhys. Lett.* **86** 67005

[137] Singh D J, Du M H, Zhang L, Subedi A and An J 2009 Electronic structure, magnetism and superconductivity of layered iron compounds *Physica* C **469** 886

[138] Mazin I I and Schmalian J 2009 Pairing symmetry and pairing state in ferropnictides: theoretical overview *Physica* C **469** 614

[139] Chubukov A V 2009 Renormalization group analysis of competing orders and the pairing symmetry in Fe-based superconductors *Physica* C **469** 640

[140] Kuroki K and Aoki H 2009 Unconventional pairing originating from disconnected Fermi surfaces in the iron-based superconductor *Physica* C **469** 635

[141] Ahilan K, Ning F L, Imai T, Sefat A S, Jin R, McGuire M A, Sales B C and Mandrus D 2008 $^{19}$F NMR investigation of the iron pnictide superconductor $LaFeAsO_{0.89}F_{0.11}$ *Phys. Rev.* B **78** 100501

[142] Nakai Y, Ishida K, Kamihara Y, Hirano M and Hosono H 2008 Evolution from itinerant antiferromagnet to unconventional superconductor with fluorine doping in $LaFeAsO_{1-x}F_x$ revealed by $^{75}$As and $^{139}$La nuclear magnetic resonance *J. Phys. Soc. Japan* **77** 073701

[143] Christianson A D *et al* 2008 Unconventional superconductivity in $Ba_{0.6}K_{0.4}Fe_2As_2$ from inelastic neutron scattering *Nature* **456** 930

[144] Lumsden M D *et al* 2009 Two-dimensional resonant magnetic excitation in $BaFe_{1.84}Co_{0.16}As_2$ *Phys. Rev. Lett.* **102** 107005

[145] Chi S X *et al* 2009 Inelastic neutron-scattering measurements of a three-dimensional spin resonance in the FeAs-based $BaFe_{1.9}Ni_{0.1}As_2$ superconductor *Phys. Rev. Lett.* **102** 107006

[146] Ewings R A, Perring T G, Bewley R I, Guidi T, Pitcher M J, Parker D R, Clarke S J and Boothroyd A T 2008 High-energy spin excitations in $BaFe_2As_2$ observed by inelastic neutron scattering *Phys. Rev.* B **78** 220501

[147] Yao D X and Carlson E W 2008 Magnetic excitations in the high-$T_C$ iron pnictides *Phys. Rev.* B **78** 052507

[148] Mcqueeney R J *et al* 2008 Anisotropic three-dimensional magnetism in $CaFe_2As_2$ *Phys. Rev. Lett.* **101** 227205

[149] Diallo S O *et al* 2009 Itinerant magnetic excitations in antiferromagnetic $CaFe_2As_2$ *Phys. Rev. Lett.* **102** 187206

[150] Zhao J, Adroja D T, Yao D X, Bewley R, Li S L, Wang X F, Wu G, Chen X H, Hu J P and Dai P C 2009 Spin waves and magnetic exchange interactions in $CaFe_2As_2$ *Nat. Phys.* **5** 555

[151] Matan K, Morinaga R, Iida K and Sato T J 2009 Anisotropic itinerant magnetism and spin fluctuations in $BaFe_2As_2$: a neutron scattering study *Phys. Rev.* B **79** 054526

[152] Diallo S O *et al* 2010 Paramagnetic spin correlations in $CaFe_2As_2$ single crystals arXiv:1001.2804v1

[153] Zhao J *et al* 2008 Low energy spin waves and magnetic interactions in $SrFe_2As_2$ *Phys. Rev. Lett.* **101** 167203

[154] Kastner M A, Birgeneau R J, Shirane G and Endoh Y 1998 Magnetic, transport, and optical properties of monolayer copper oxides *Rev. Mod. Phys.* **70** 897

[155] Fukazawa H *et al* 2009 Possible multiple gap superconductivity with line nodes in heavily hole-doped superconductor $KFe_2As_2$ studied by $^{75}$As nuclear quadrupole resonance and specific heat *J. Phys. Soc. Japan* **78** 083712

[156] Han M J, Yin Q, Pickett W E and Savrasov S Y 2009 Anisotropy, itineracy, and magnetic frustration in high-$T_C$ iron pnictides *Phys. Rev. Lett.* **102** 107003

[157] Ishikado M *et al* 2009 Two-dimensional spin density wave state in LaFeAsO *J. Phys. Soc. Japan* **78** 043705

[158] Chi S *et al* 2008 Crystalline electric field as a probe for long-range antiferromagnetic order and superconducting state of $CeFeAsO_{1-x}F_x$ *Phys. Rev. Lett.* **101** 217002

[159] Iikubo S, Fujita M, Niitaka S and Takagi H 2009 Antiferromagnetic fluctuations in $Fe(Se_{1-x}Te_x)_{0.92}$ ($x = 0.75$, 1) observed by inelastic neutron scattering *J. Phys. Soc. Japan* **78** 103704

[160] Inosov D S *et al* 2010 Normal-state spin dynamics and temperature-dependent s pin-resonance energy in optimally doped $BaFe_{1.85}Co_{0.15}As_2$ *Nat. Phys.* **6** 178

[161] Matan K, Ibuka S, Morinaga R, Chi S, Lynn J W, Christianson A D, Lumsden M D and Sato T J 2009 Doping dependence of spin dynamics in electron-doped $Ba(Fe_{1-x}Co_x)_2As_2$ arXiv:0912.4945

[162] Lester C, Chu J H, Analytis J G, Perring T G, Fisher I R and Hayden S M 2010 Disperive spin fluctuations in the nearly optimally doped superconductor $Ba(Fe_{1-x}Co_x)_2As_2$ ($x = 0.065$) *Phys. Rev.* B **81** 064505

[163] Moriya T 1985 *Spin Fluctuations in Itinerant Electron Magnetism* (*Springer Series in Solid State Sciences*) (Berlin: Springer)

[164] Fong H F, Bourges P, Sidis Y, Regnault L P, Bossy J, Ivanov A, Milius D L, Aksay I A and Keimer B 2000 Spin susceptibility in underdoped $YB_2Cu_3O_{6+x}$ *Phys. Rev.* B **61** 14773

[165] Ning F L, Ahilan K, Imai T, Sefat A S, McGuire M A, Sales B C, Mandrus D, Cheng P, Shen B and Wen H-H 2010 Contrasting spin dynamics between underdoped and overdoped $Ba(Fe_{1-x}Co_x)_2As_2$ *Phys. Rev. Lett.* **104** 037001

[166] Brouet V, Marsi M, Mansart B, Nicolaou A, Taleb-Ibrahimi A, Le Fèvre P, Bertran F, Rullier-Albenque F, Forget A and Colson D 2009 Nesting between hole and electron pockets in $Ba(Fe_{1-x}Co_x)_2As_2$ ($x = 0$–0.3) observed with angle-resolved photoemission *Phys. Rev.* B **80** 165115

[167] Zhang S W, Ma L, Hou Y D, Zhang J, Xia T-L, Chen G F, Hu J P, Luke G M and Yu W 2010 $^{75}$As NMR study of single crystals of the heavily overdoped pnictide superconductors $Ba_{1-x}K_xFe_2As_2$ ($x = 0.7$ and 1) *Phys. Rev.* B **81** 012503

[168] Wakimoto S *et al* 2009 Degradation of superconductivity and spin fluctuations by electron over-doping in $LaFeAsO_{1-x}F_x$ arXiv:0906.2453v2

[169] Torikachvili M S, Bud'ko S L, Ni N and Canfield P C 2008 Pressure induced superconductivity in $CaFe_2As_2$ *Phys. Rev. Lett.* **101** 057006

[170] Park T, Park E, Lee H, Klimczuk T, Bauer E D, Ronning F and Thompson J D 2008 Pressure-induced superconductivity in $CaFe_2As_2$ *J. Phys.: Condens. Matter* **20** 322204

[171] Yu W, Aczel A A, Williams T J, Bud'ko S L, Ni N, Canfield P C and Luke G M 2009 Absence of superconductivity in single-phase $CaFe_2As_2$ under hydrostatic pressure *Phys. Rev.* B **79** 020511

[172] Pratt D K *et al* 2009 Suppression of antiferromagnetic spin fluctuations in the collapsed phase of $CaFe_2As_2$ *Phys. Rev.* B **79** 060510

[173] Goldman A I *et al* 2009 Lattice collapse and quenching of magnetism in $CaFe_2As_2$ under pressure: a single-crystal neutron and x-ray diffraction investigation *Phys. Rev.* B **79** 024513

[174] Mook H A *et al* 2009 Neutron scattering patterns show Superconductivity in $FeTe_{0.5}Se_{0.5}$ likely results from itinerant electron fluctuations arXiv:0904.2178

[175] Qiu Y M *et al* 2009 Spin gap and resonance at the nesting wave vector in superconducting $FeSe_{0.4}Te_{0.6}$ *Phys. Rev. Lett.* **103** 067008

[176] Lumsden M D *et al* 2010 Evolution of spin excitations into the superconducting state in $FeTe_{1-x}Se_x$ *Nat. Phys.* **6** 182

[177] Argyriou D N *et al* 2009 Incommensurate itinerant antiferromagnetic excitations and spin resonance in the $FeTe_{0.6}Se_{0.4}$ superconductor arXiv:0911.4713v1

[178] Mook H A *et al* 2009 Unusual relationship between magnetism and superconductivity in $FeTe_{0.5}Se_{0.5}$ arXiv:0911.5463

[179] Lee S-H *et al* 2009 Coupling of spin and orbital excitations in an Fe-based superconductor arXiv:0912.3205v1

[180] Li H-F *et al* 2010 Anisotropic and quasi-propagating spin excitations in optimally-doped superconducting $Ba(Fe_{0.926}Co_{0.074})_2As_2$ arXiv:1003.1687v1

[181] Vignolle B *et al* 2007 Two energy scales in the spin excitations of the high-temperature superconductor $La_{2-x}Sr_xCuO_4$ *Nature Phys.* **3** 163

[182] Monthoux P and Scalapino D J 1994 Self-consistent $d_{x^2-y^2}$ pairing in a two-dimensional Hubbard model *Phys. Rev. Lett.* **72** 1874

[183] Fong H F, Keimer B, Anderson P W, Reznik D, Dogan F and Aksay I A 1995 Phonon and magnetic neutron scattering at 41 meV in $YBa_2Cu_3O_7$ *Phys. Rev. Lett.* **75** 316

[184] Batista C D, Ortiz G and Balatsky A V 2001 Unified description of the resonance peak and incommensuration in high-$T_C$ superconductors *Phys. Rev.* B **64** 172508

[185] Lee P A and Nagaosa N 2006 Doping a Mott insulator: physics of high-temperature superconductivity *Rev. Mod. Phys.* **78** 17

[186] Chang Jun, Eremin I, Thalmeier P and Fulde P 2007 Theory of magnetic excitons in the heavy-fermion superconductor $UPd_2Al_3$ *Phys. Rev.* B **75** 024503

[187] Norman M R 2007 Linear response theory and the universal nature of the magnetic excitation spectrum of the cuprates *Phys. Rev.* B **75** 184514

[188] Rossat-Mignod J, Regnault L P, Vettier C, Bourges P, Burlet P, Bossy J, Henry J Y and Lapertot G 1991 Neutron scattering study of the $YBa_2Cu_3O_{6+x}$ system *Physica* C **185–189** 86

[189] Mook H A, Yethiraj M, Aeppli G, Mason T E and Armstrong T 1993 Polarized neutron determination of the magnetic excitations in $YBa_2Cu_3O_7$ *Phys. Rev. Lett.* **70** 3490–3

[190] Fong H F, Bourges P, Sidis Y, Regnault L P, Ivanov A, Gu G D, Koshizuka N and Keimer B 1999 Neutron scattering from magnetic excitations in $Bi_2Sr_2CaCu_2O_{8+\delta}$ *Nature* **398** 588

[191] Dai P, Mook H A, Aeppli G, Hayden S M and Dogan F 2000 Resonance as a measure of pairing correlations in the high-$T_C$ superconductor $YBa_2Cu_3O_{6.6}$ *Nature* **406** 965

[192] Sato N K, Aso N, Miyake K, Shiina R, Thalmeier P, Varelogiannis G, Geibel C, Steglich F, Fulde P and Komatsubara T 2001 Strong coupling of magnetic excitons and heavy quasiparticles in $UPd_2Al_3$ *Nature* **410** 340

[193] Stock C, Broholm C, Hudis J, Kang H J and Petrovic C 2008 Spin resonance in the d-wave superconductor $CeCoIn_5$ *Phys. Rev. Lett.* **100** 087001

[194] Li S L, Chen Y, Chang S, Lynn J W, Li L J, Luo Y K, Cao G H, Xu Z A and Dai P C 2009 Spin gap and magnetic resonance in superconducting $BaFe_{1.9}Ni_{0.1}As_2$ *Phys. Rev.* B **79** 174527

[195] Parshall D *et al* 2009 Spin excitations in $BaFe_{1.84}Co_{0.16}As_2$ superconductor observed by inelastic neutron scattering *Phys. Rev.* B **80** 012502

[196] Wen J, Xu G, Xu Z, Lin Z W, Li Q, Chen Y, Chi S, Gu G and Tranquada J M 2010 Magnetic field effect on the spin resonance in $FeTe_{0.5}Se_{0.5}$ ($T_C = 14$ K) *Phys. Rev.* B **81** 100513(R)

[197] Shamoto S 2010 private communication

[198] Osborn R, Rosenkranz S, Goremychkin E A and Christianson A D 2009 Inelastic neutron scattering studies of the spin and lattice dynamics in iron arsenide compounds *Physica* C **469** 498

[199] Yashima M, Nishimura H, Mukuda H, Kitaoka Y, Miyazawa K, Shirage P M, Kihou K, Kito H, Eisaki H and Iyo A 2009 Strong-coupling spin-singlet superconductivity with multiple full gaps in hole-doped $Ba_{0.6}K_{0.4}Fe_2As_2$ probed by $^{57}$Fe NMR *J. Phys. Soc. Japan* **78** 103702

[200] Terashima K *et al* 2009 Fermi surface nesting induced strong pairing in iron-based superconductors *Proc. Natl Acad. Sci. USA* **106** 7330

[201] Ding H *et al* 2008 Observation of Fermi-surface-dependent nodeless superconducting gaps in $Ba_{0.6}K_{0.4}Fe_2As_2$ *Europhys. Lett.* **83** 47001

[202] Samuely P, Pribulova Z, Szabo P, Pristas G, Bud'ko S L and Canfield P C 2009 Point contact Andreev reflection spectroscopy of superconducting energy gaps in 122-type family of iron pnictides *Physica* C **469** 507

[203] Yin Y, Zech M, Williams T L and Hoffman J E 2009 Scanning tunneling microscopy and spectroscopy on iron-pnictides *Physica* C **469** 535

[204] Tranquada J M, Lee C H, Yamada K, Lee Y S, Regnault L P and Ronnow H M 2004 Evidence for an incommensurate magnetic resonance in $La_{2-x}Sr_xCuO_4$ *Phys. Rev.* B **69** 174507

[205] Zhao J, Regnault L-P, Zhang C, Wang M, Li Z, Zhao F, Zhao Z and Dai P 2009 Resonance as a probe of the electron superconducting gap in $BaFe_{1.9}Ni_{0.1}As_2$ arXiv:0908.0954

[206] Bao W, Savici A T, Granroth G E, Broholm C, Habicht K, Qiu Y, Hu J, Liu T and Mao Z Q 2010 A triplet resonance in superconducting $FeSe_{0.4}Te_{0.6}$ arXiv:1002.1617v1

[207] Hüfner S, Hossain M A, Damascelli A and Sawatzky G A 2008 *Rep. Prog. Phys.* **71** 062501

[208] Mourachkine A 1999 The order parameters for pairing and phase coherence in cuprates; the magnetic origin of the coherent gap. The MCS model of high-$T_C$ superconductivity *J. Low Temp. Phys.* **117** 401

[209] Yu G, Li Y, Motoyama E M and Greven M 2009 A universal relationship between magnetic resonance and superconducting gap in unconventional superconductors *Nat. Phys.* **5** 873

[210] Kuroki K, Onari S, Arita R, Usui H, Tanaka Y, Kontani H and Aoki H 2008 Unconventional pairing originating from the disconnected Fermi surfaces of superconducting $LaFeAsO_{1-x}F_x$ *Phys. Rev. Lett.* **101** 087004

[211] Maier T A and Scalapino D J 2008 Theory of neutron scattering as a probe of the superconducting gap in the iron pnictides *Phys. Rev.* B **78** 020514

[212] Korshunov M M and Eremin I 2008 Theory of magnetic excitations in iron-based layered superconductors *Phys. Rev.* B **78** 140509

[213] Maier T A, Graser S, Scalapino D J and Hirschfeld P 2009 Neutron scattering resonance and the iron-pnictide superconducting gap *Phys. Rev.* B **79** 134520

[214] Onari S, Kontani H and Sato M 2010 Neutron-scattering peak in both $s_{++}$ wave and $s_{+-}$ wave states of an iron pnictide superconductor *Phys. Rev.* B **81** 060504(R)